PATIENT-SPECIFIC DYNAMIC MODELING TO PREDICT FUNCTIONAL OUTCOMES

By

JEFFREY A. REINBOLT

A DISSERTATION PRESENTED TO THE GRADUATE SCHOOL
OF THE UNIVERSITY OF FLORIDA IN PARTIAL FULFILLMENT
OF THE REQUIREMENTS FOR THE DEGREE OF
DOCTOR OF PHILOSOPHY

UNIVERSITY OF FLORIDA

2006

This dissertation is dedicated to my loving wife, Karen, and our wonderful son, Jacob.

ACKNOWLEDGMENTS

I sincerely thank Dr. B. J. Fregly for his support and leadership throughout our research endeavors; moreover, I truly recognize the value of his honest, straightforward, and experience-based advice. My life has been genuinely influenced by Dr. Fregly's expectations, confidence, and trust in me.

I also extend gratitude to Dr. Raphael Haftka, Dr. Carl Crane, Dr. Scott Banks, and Dr. Steven Kautz for their dedication, knowledge, and instruction both inside and outside of the classroom. For these reasons, each was selected to serve on my supervisory committee. I express thanks to all four individuals for their time, contribution, and fulfillment of their committee responsibilities.

I collectively show appreciation for my family, friends, and colleagues. Unconditionally, they have provided me with encouragement, support, and interest in my graduate studies and research activities.

My wife, Karen, has done more for me than any person could desire. On several occasions, she has taken a leap of faith with me; more importantly, she has been directly beside me. Words or actions cannot adequately express my gratefulness and adoration toward her. I honestly hope that I can provide her as much as she has given to me.

I thank God for my excellent health, inquisitive mind, strong faith, valuable experiences, encouraging teachers, loving family, supportive friends, and remarkable wife.

TABLE OF CONTENTS

LIST OF TABLES

LIST OF FIGURES

Abstract of Dissertation Presented to the Graduate School
of the University of Florida in Partial Fulfillment of the
Requirements for the Degree of Doctor of Philosophy

PATIENT-SPECIFIC DYNAMIC MODELING
TO PREDICT FUNCTIONAL OUTCOMES

By

Jeffrey A. Reinbolt

May 2006

Chair: Benjamin J. Fregly
Major Department: Mechanical and Aerospace Engineering

Movement related disorders have treatments (e.g., corrective surgeries, rehabilitation) generally characterized by variable outcomes as a result of subjective decisions based on qualitative analyses using a one-size-fits-all healthcare approach. Imagine the benefit to the healthcare provider and, more importantly, the patient, if certain clinical parameters may be evaluated pre-treatment in order to predict the post-treatment outcome. Using patient-specific models, movement related disorders may be treated with reliable outcomes as a result of objective decisions based on quantitative analyses using a patient-specific approach.

The general objective of the current work is to predict post-treatment outcome using patient-specific models given pre-treatment data. The specific objective is to develop a four-phase optimization approach to identify patient-specific model parameters and utilize the calibrated model to predict functional outcome. Phase one involves identifying joint parameters describing the positions and orientations of joints within

adjacent body segments. Phase two involves identifying inertial parameters defining the mass, centers of mass, and moments of inertia for each body segment. Phase three involves identifying control parameters representing weighted components of joint torque inherent in different walking movements. Phase four involves an inverse dynamics optimization to predict function outcome. This work comprises a computational framework to create and apply patient-specific models to predict clinically significant outcomes.

CHAPTER 1
INTRODUCTION

Arthritis: The Nation's Leading Cause of Disability

In 1997, the Centers for Disease Control and Prevention (CDC) reported that 43 million (or 1 in 6) Americans suffered with arthritis. A 2002 CDC study showed that 70 million (a 63% increase in 5 years; or 1 in 3) Americans have arthritis (CDC, 2003). Approximately two-thirds of individuals with arthritis are under 65 years old. As the population ages, the number of people with arthritis is likely to increase significantly. The most common forms of arthritis are osteoarthritis, rheumatoid arthritis, fibromyalgia, and gout. Osteoarthritis of the knee joint accounts for roughly 30% ($25 billion) of the $82 billion total arthritis costs per year in the United States.

Knee osteoarthritis symptoms of pain and dysfunction are the primary reasons for total knee replacement (TKR). This procedure involves a resurfacing of bones surrounding the knee joint. The end of the femur is removed and covered with a metal implant. The end of the tibia is removed and substituted by a plastic implant. Smooth metal and plastic articulation replaces the irregular and painful arthritic surfaces. Approximately 100,000 Medicare patients alone endure TKR procedures each year (Heck *et al.*, 1998). Hospital charges for unilateral TKR are more than $30,000 and the cost of bilateral TKR is over $50,000 (Lane *et al.*, 1997).

An alternative to TKR is a more conservative (both economically and surgically) corrective procedure known as high tibial osteotomy (HTO). By changing the frontal plane alignment of the tibia with a wedge of bone, a HTO shifts the weight-bearing axis

of the leg, and thus the mechanical stresses, from the diseased portion to the healthy section of the knee compartment. By transferring the location of mechanical stresses, the degenerative disease process may be slowed or possibly reversed. The advantages of HTO are appealing to younger and active patients who receive recommendations to avoid TKR.

Need for Patient-Specific Simulations

Innovative patient-specific models and simulations would be valuable for addressing problems in orthopedics and sports medicine, as well as for evaluating and enhancing corrective surgical procedures (Arnold *et al.*, 2000; Arnold and Delp, 2001; Chao *et al.*, 1993; Chao and Sim, 1995; Delp *et al.*, 1998; Delp *et al.*, 1996; Delp *et al.*, 1990; Pandy, 2001). For example, a patient-specific dynamic model may be useful for planning intended surgical parameters and predicting the outcome of HTO.

The main motivation for developing the following patient-specific dynamic model and the associated multi-phase optimization approach is to predict the post-surgery peak internal knee abduction moment in HTO patients. Conventional surgical planning techniques for HTO involve choosing the amount of necessary tibial angulation from standing radiographs (or x-rays). Unfortunately, alignment correction estimates from static x-rays do not accurately predict long-term clinical outcome after HTO (Andriacchi, 1994; Tetsworth and Paley, 1994). Researchers have identified the peak external knee adduction moment as an indicator of clinical outcome while investigating the gait of HTO patients (Andriacchi, 1994; Bryan *et al.*, 1997; Hurwitz *et al.*, 1998; Prodromos *et al.*, 1985; Wang *et al.*, 1990). Currently, no movement simulations (or other methods for that matter) allow surgeons to choose HTO surgical parameters to achieve a chosen post-surgery knee abduction moment.

The precision of dynamic analyses is fundamentally associated with the accuracy of kinematic and kinetic model parameters (Andriacchi and Strickland, 1985; Challis and Kerwin, 1996; Cappozzo and Pedotti, 1975; Davis, 1992; Holden and Stanhope, 1998; Holden and Stanhope, 2000; Stagni *et al.*, 2000). Understandably, a model constructed of rigid links within a multi-link chain and simple mechanical approximations of joints will not precisely match the human anatomy and function. The model should provide the best possible agreement to experimental motion data within the bounds of the dynamic model selected (Sommer and Miller, 1980).

Background

Motion Capture

Motion capture is the use of external devices to capture the movement of a real object. One type of motion-capture technology is based on a passive optical technique. Passive refers to markers, which are simply spheres covered in reflective tape, placed on the object. Optical refers to the technology used to provide 3D data, which involves high-speed, high-resolution video cameras. By placing passive markers on an object, special hardware records the position of those markers in time and it generates a set of motion data (or marker data).

Often motion capture is used to create synthetic actors by capturing the motions of real humans. Special effects companies have used this technique to produce incredibly realistic animations in movies such as *Star Wars Episode I & II*, *Titanic*, *Batman*, and *Terminator 2*.

Biomechanical Models

Researchers use motion-capture technology to construct biomechanical models of the human structure. The position of external markers may be used to estimate the

position of internal landmarks such as joint centers. The markers also enable the creation of individual segment reference frames that define the position and orientation of each body segment within a Newtonian laboratory reference frame. Marker data collected from an individual are used to prescribe the motion of the biomechanical model.

Kinematics and Dynamics

Human kinematics is the study of the positions, angles, velocities, and accelerations of body segments and joints during motion. With kinematic data and mass-distribution data, one can study the forces and torques required to produce the recorded motion data. Errors between the biomechanical model and the recorded motion data will inevitably propagate to errors in the force and torque results of dynamic analyses.

Optimization

Optimization involves searching for the minimum or maximum of an objective function by adjusting a set of design variables. For example, the objective function may be the errors between the biomechanical model and the recorded data. These errors are a function of the model's generalized coordinates and the model's kinematic and kinetic parameters. Optimization may be used to modify the design variables of the model to minimize the overall fitness errors and identify a structure that matches the experimental data very well.

CHAPTER 2
CREATION OF PATIENT-SPECIFIC DYNAMIC MODELS FROM THREE-DIMENSIONAL MOVEMENT DATA USING OPTIMIZATION

Background

Forward and inverse dynamics analyses of gait can be used to study clinical problems in neural control, rehabilitation, orthopedics, and sports medicine. These analyses utilize a dynamic skeletal model that requires values for joint parameters (JPs - joint positions and orientations in the body segments) and inertial parameters (IPs - masses, mass centers, and moments of inertia of the body segments). If the specified parameter values do not match the patient's anatomy and mass distribution, then the predicted gait motions and loads may not be indicative of the clinical situation.

The literature contains a variety of methods to estimate JP and IP values on a patient-specific basis. Anatomic landmark methods estimate parameter values using scaling rules developed from cadaver studies (Bell *et al.*, 1990; Churchill *et al.*, 1998; Inman, 1976; de Leva, 1996). In contrast, optimization methods adjust parameter values to minimize errors between model predictions and experimental measurements. Optimizations identifying JP values for three-dimensional (3D) multi-joint kinematic models have a high computational cost (Reinbolt *et al.*, 2005). Optimizations identifying IP values without corresponding optimizations identifying JP values have been performed with limited success for planar models of running, jumping, and kicking motions (Vaughan *et al.*, 1982).

This study presents a computationally-efficient two-phase optimization approach for determining patient-specific JP and IP values in a dynamic skeletal model given experimental movement data to match. The first phase determines JP values that best match experimental kinematic data, while the second phase determines IP values that best match experimental kinetic data. The approach is demonstrated by fitting a 3D, 27 degree-of-freedom (DOF), parametric full-body gait model possessing 98 JPs and 84 IPs to synthetic (i.e., computer generated) and experimental movement data.

Methods

A sample dynamic model is needed to demonstrate the proposed two-phase optimization approach. For this purpose, a parametric 3D, 27 DOF, full-body gait model whose equations of motion were derived with the symbolic manipulation software, Autolev™ (OnLine Dynamics, Sunnyvale, CA), was used (Figure 2-1, Table 2-1). Comparable to Pandy's (2001) model structure, 3 translational and 3 rotational DOFs express the movement of the pelvis in a Newtonian reference frame and the remaining 13 segments comprised four open chains branching from the pelvis. The positions and orientations of joint axes within adjacent segment coordinate systems were defined by unique JPs. For example, the knee joint axis is simultaneously established in the femur and tibia coordinate systems. These parameters are used to designate the geometry of the following joint types: 3 DOF hip, 1 DOF knee, 2 DOF ankle, 3 DOF back, 2 DOF shoulder, and 1 DOF elbow. Each joint provides a simplified mechanical approximation to the actual anatomic articulations. Anatomic landmark methods were used to estimate nominal values for 6 hip (Bell *et al.*, 1990), 9 knee (Churchill *et al.*, 1998), and 12 ankle (Inman, 1976) JPs (Figure 2-2, Table 2-2, Figure 2-3, Table 2-3, Figure 2-4, Table 2-4). The segment masses, mass centers, and moments of inertia were described by unique IPs.

Anatomic landmark methods were used to estimate nominal values for 7 IPs per segment (de Leva, 1996).

Parameters defining the structure of the model were referenced to local coordinate systems fixed in each body segment. These coordinate systems were created from a static motion capture trial (see below). Markers placed over the left anterior superior iliac spine (ASIS), right ASIS, and superior sacrum were used to define the pelvis segment coordinate system (Figure 2-2). From percentages of the inter-ASIS distance, a nominal hip joint center location was estimated within the pelvis segment (Bell *et al.*, 1990). This nominal joint center served as the origin of the femur coordinate system, which was subsequently defined using markers placed over the medial and lateral femoral epicondyles (Figure 2-2). The tibia coordinate system originated at the midpoint of the knee markers and was defined by additional markers located on the medial and lateral malleoli (Figure 2-3). The talus coordinate system was created where the y-axis extends along the line perpendicular to both the talocrural joint axis and the subtalar joint axis (Figure 2-4). The heel and toe markers, in combination with the tibia y-axis, defined the foot coordinate system (Figure 2-4).

Experimental kinematic and kinetic data were collected from a single subject using a video-based motion analysis system (Motion Analysis Corporation, Santa Rosa, CA) and two force plates (AMTI, Watertown, MA). Institutional review board approval and informed consent were obtained prior to the experiments. As described above, segment coordinate systems were created from surface marker locations measured during a static standing pose (Figure 2-5). Unloaded isolated joint motions were performed to exercise the primary functional axes of each lower extremity joint (hip, knee, and ankle on each

side). For each joint, the subject was instructed to move the distal segment within the physiological range of motion so as to exercise all DOFs of the joint. Three trials were done for each joint with all trials performed unloaded. Multiple cycles of standing hip flexion-extension followed by abduction-adduction were recorded. Similar to Leardini *et al.* (1999), internal-external rotation of the hip was avoided to reduce skin and soft tissue movement artifacts. Multiple cycles of knee flexion-extension were measured. Finally, multiple cycles of simultaneous ankle plantarflexion-dorsiflexion and inversion-eversion were recorded. Gait motion and ground reaction data were collected to investigate simultaneous motion of all lower extremity joints under load-bearing physiological conditions.

To evaluate the proposed optimization methodology, two types of synthetic movement data were generated from the experimental data sets. The first type was noiseless synthetic data generated by moving the model through motions representative of the isolated joint and gait experiments. The second type was synthetic data with superimposed numerical noise to simulate skin and soft tissue movement artifacts. A continuous noise model of the form $A\sin(\omega t + \varphi)$ was used with the following uniform random parameter values: amplitude ($0 \le A \le 1$ cm), frequency ($0 \le \omega \le 25$ rad/s), and phase angle ($0 \le \varphi \le 2\pi$) (Chèze *et al.*, 1995).

The first phase of the optimization procedure adjusted JP values and model motion to minimize errors between model and experimental marker locations (Equation 2-1, Figure 2-6). For isolated joint motion trials, the design variables were 540 B-spline nodes (q) parameterizing the generalized coordinate trajectories (20 nodes per DOF) and 6 hip, 9 knee, or 12 ankle JPs ($\boldsymbol{p}_{JP}$). For the gait trial, the number of JPs was reduced to 4

hip, 9 knee, and 4 ankle, due to inaccuracies in determining joint functional axes with rotations less than 25° (Chèze *et al.*, 1998). The initial value for each B-spline node and JP was chosen to be zero to test the robustness of the optimization approach. The JP cost function (e_{JP}) minimized the errors between model (m') and experimental (m) marker locations for each of the 3 marker coordinates over *nm* markers and *nf* time frames. The JP optimizations were performed with Matlab's nonlinear least squares algorithm (The Mathworks, Natick, MA).

$$e_{JP} = \min_{p_{JP},q} \sum_{i=1}^{nf} \sum_{j=1}^{nm} \sum_{k=1}^{3} \left[m_{ijk} - m'_{ijk}(p_{JP}, q) \right]^2 \tag{2-1}$$

The second phase of the optimization procedure adjusted IP values to minimize the residual forces and torques acting on a 6 DOF ground-to-pelvis joint (Equation 2-2, Figure 2-7). Only the gait trial was used in this phase. The design variables for phase two were a reduced set of 20 IPs (p_{IP} – 7 masses, 8 centers of mass, and 5 moments of inertia) accounting for body symmetry and limited joint ranges of motion during gait. The initial seed for each IP was the nominal value or a randomly altered value within ± 50% of nominal. The IP cost function (e_{IP}) utilized a combination of pelvis residual loads (F and T) calculated over all *nf* time frames and differences between initial (p'_{IP}) and current (p_{IP}) IP values. The residual pelvis forces (F) were normalized by body weight (BW) and the residual pelvis torques (T) by body weight times height ($BW*H$). IP differences were normalized by their respective initial values to create nondimensional errors. The IP optimizations also were performed with Matlab's nonlinear least squares algorithm. Once a IP optimization converged, the final IP values were used as the initial

guess for a subsequent IP optimization, with this processing being repeated until the resulting pelvis residual loads converged.

$$\boldsymbol{e}_{IP} = \min_{\boldsymbol{p}_{IP}} \sum_{i=1}^{nf} \sum_{j=1}^{3} \left\{ \left[\frac{F_{ij}(\boldsymbol{p}_{IP})}{BW} \right]^2 + \left[\frac{T_{ij}(\boldsymbol{p}_{IP})}{BW * H} \right]^2 \right\} + \left(\frac{\boldsymbol{p}_{IP} - \boldsymbol{p'}_{IP}}{\boldsymbol{p'}_{IP}} \right)^2 \quad (2\text{-}2)$$

The JP and IP optimization procedures were applied to all three data sets (i.e., synthetic data without noise, synthetic data with noise, and experimental data). For isolated joint motion trials, JPs for each joint were determined through separate optimizations. For comparison, JPs for all three joints were determined simultaneously for the gait trial. Subsequently, IPs were determined for the gait trial using the previously optimum JP values. Root-mean-square (RMS) errors between original and recovered parameters, marker distances, and pelvis residual loads were used to quantify the procedure's performance. All optimizations were performed on a 3.4 GHz Pentium 4 PC.

Results

For phase one, each JP optimization using noiseless synthetic data precisely recovered the original marker trajectories and model parameters to within an arbitrarily tight convergence tolerance (Table 2-5, Table 2-6). For the other two data sets, RMS marker distance errors were at most 6.62 mm (synthetic with noise) and 4.04 mm (experimental), which are of the same order of magnitude as the amplitude of the applied continuous noise model. Differences between experimental data results and anatomic landmark methods are much larger than differences attributed to noise alone for synthetic data with noise (Table 2-7). Optimizations involving the isolated joint trial data sets (i.e., 1200 time frames of data) required between 108 and 380 seconds of CPU time while the gait trial data set (i.e., 208 time frames of data) required between 70 and 100 seconds of

CPU time. These computation times were orders of magnitude faster than those reported using a two-level optimization procedure (Reinbolt *et al.*, 2005).

For phase two, each IP optimization using noiseless synthetic data produced zero pelvis residual loads and recovered the original IP values to within an arbitrarily tight convergence tolerance (Table 2-8, Table 2-9). For the other two data sets, pelvis residual loads and IP errors remained small, with a random initial seed producing nearly the same pelvis residual loads but slightly higher IP errors than when the correct initial seed was used. Differences between experimental data results and anatomic landmark methods are small compared to differences attributed to noise and initial seed for synthetic data with noise (Table 2-10). Required CPU time ranged from 11 to 48 seconds.

Discussion

The accuracy of dynamic analyses of a particular patient depends on the accuracy of the associated kinematic and kinetic model parameters. Parameters are typically estimated from anatomic landmark methods. The estimated (or nominal) values may be improved by formulating a two-phase optimization problem driven by motion capture data. Optimized dynamic models can provide a more reliable foundation for future patient-specific dynamic analyses and optimizations.

This study presented a two-phase optimization approach for tuning joint and inertial parameters in a dynamic skeletal model to match experimental movement data from a specific patient. For the full-body gait model used in this study, the JP optimization satisfactorily reproduced patient-specific JP values while the IP optimization successfully reduced pelvis residual loads while allowing variation in the IP values away from their initial guesses. The JP and IP values found by this two-phase optimization approach are only as reliable as the noisy experimental movement data used

as inputs. By optimizing over all time frames simultaneously, the procedure smoothes out the effects of this noise. An optimization approach that modifies JPs and IPs simultaneously may provide even further reductions in pelvis residual loads.

It cannot be claimed that models fitted with this two-phase approach will reproduce the actual functional axes and inertial properties of the patient. This is clear from the results of the synthetic data with noise, where the RMS errors in the recovered parameters were not zero. At the same time, the optimized parameters for this data set corresponded to a lower cost function value in each case than did the nominal parameters from which the synthetic data were generated. Thus, it can only be claimed that the optimized model structure provides the best possible fit to the imperfect movement data.

There are differences between phase one and phase two when comparing results for experimental data to synthetic data with noise. For the JP case, absolute parameter differences were higher for experimental data compared to synthetic data with noise. This suggests that noise does not hinder the process of determining JPs. However, for the IP case, absolute parameter differences were higher for synthetic data with noise compared to experimental data. In fact, noise is a limiting factor when identifying IPs.

The phase one optimization determined patient-specific joint parameters similar to previous works. The optimal hip joint center location of 2.94 cm (12.01% posterior), 9.21 cm (37.63% inferior), and 9.09 cm (37.10% lateral) is comparable to 19.30%, 30.40%, and 35.90%, respectively, of the inter- ASIS distance (Bell *et al.*, 1990). The optimum femur length (42.23 cm) and tibia length (38.33 cm) are similar to 41.98 cm and 37.74 cm, respectively (de Leva, 1996). The optimum coronal plane rotation (87.36°) of the talocrural joint correlates to 82.7 ± 3.7° (range 74° to 94°) (Inman, 1976). The optimum

distance (0.58 cm) between the talocrural joint and the subtalar joint is analogous to 1.24 ± 0.29 cm (Bogert *et al.*, 1994). The optimum transverse plane rotation (34.79°) and sagittal plane rotation (31.34°) of the subtalar joint corresponds to 23 ± 11° (range 4° to 47°) and 42 ± 9° (range 20.5° to 68.5°), respectively (Inman, 1976). Compared to anatomic landmark methods reported in the literature, the phase one optimization reduced RMS marker distance errors by 17% (hip), 52% (knee), 68% (ankle), and 34% (full leg).

The phase two optimization determined patient-specific inertial parameters similar to previous work. The optimum masses were within an average of 1.99% (range 0.078% to 8.51%), centers of mass within range 0.047% to 5.84% (mean 1.58%), and moments of inertia within 0.99% (0.0038% to 5.09%) from the nominal values (de Leva, 1996). Compared to anatomic landmark methods reported in the literature, the phase two optimization reduced RMS pelvis residual loads by 20% (forces) and 8% (torques).

Two conclusions may be drawn from these comparisons. First, the similarities suggest the results are reasonable and show the extent of agreement with past studies. Second, the differences between values indicate the extent to which tuning the parameters to the patient via optimization methods would change their values compared to anatomic landmark methods. In all cases, the two-phase optimization successfully reduced cost function values for marker distance errors or pelvis residual loads below those resulting from anatomic landmark methods.

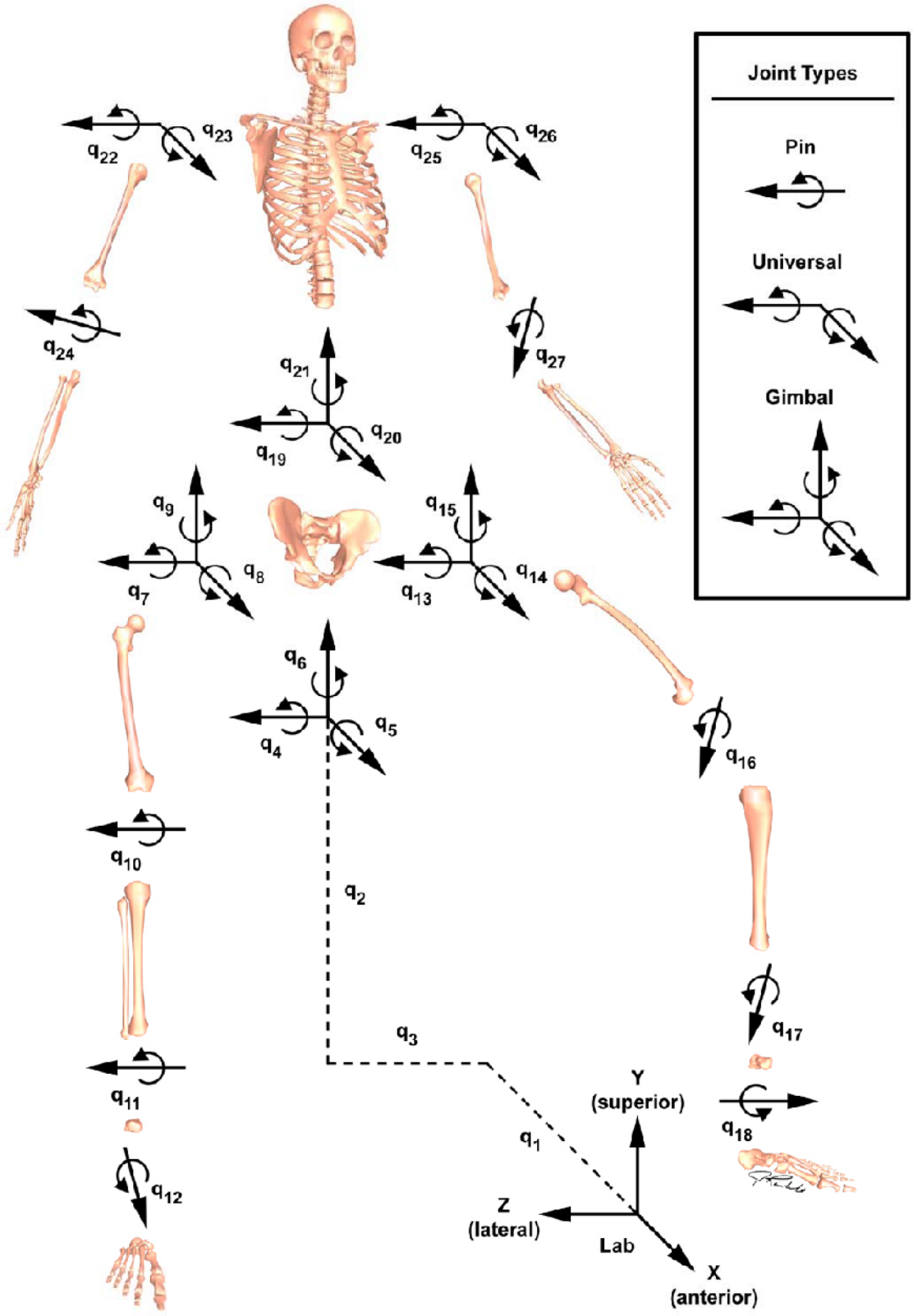

Figure 2-1. Illustration of the 3D, 14 segment, 27 DOF full-body kinematic model linkage joined by a set of gimbal, universal, and pin joints.

Table 2-1. Descriptions of the model degrees of freedom.

DOF	Description
q_1	Pelvis anterior-posterior position.
q_2	Pelvis superior-inferior position.
q_3	Pelvis medial-lateral position.
q_4	Pelvis anterior-posterior tilt angle.
q_5	Pelvis elevation-depression angle.
q_6	Pelvis internal-external rotation angle.
q_7	Right hip flexion-extension angle.
q_8	Right hip adduction-abduction angle.
q_9	Right hip internal-external rotation angle.
q_{10}	Right knee flexion-extension angle.
q_{11}	Right ankle plantarflexion-dorsiflexion angle.
q_{12}	Right ankle inversion-eversion angle
q_{13}	Left hip flexion-extension angle.
q_{14}	Left hip adduction-abduction angle.
q_{15}	Left hip internal-external rotation angle.
q_{16}	Left knee flexion-extension angle.
q_{17}	Left ankle plantarflexion-dorsiflexion angle.
q_{18}	Left ankle inversion-eversion angle
q_{19}	Trunk anterior-posterior tilt angle.
q_{20}	Trunk elevation-depression angle.
q_{21}	Trunk internal-external rotation angle.
q_{22}	Right shoulder flexion-extension angle.
q_{23}	Right shoulder adduction-abduction angle.
q_{24}	Right elbow flexion angle.
q_{25}	Left shoulder flexion-extension angle.
q_{26}	Left shoulder adduction-abduction angle.
q_{27}	Left elbow flexion angle.

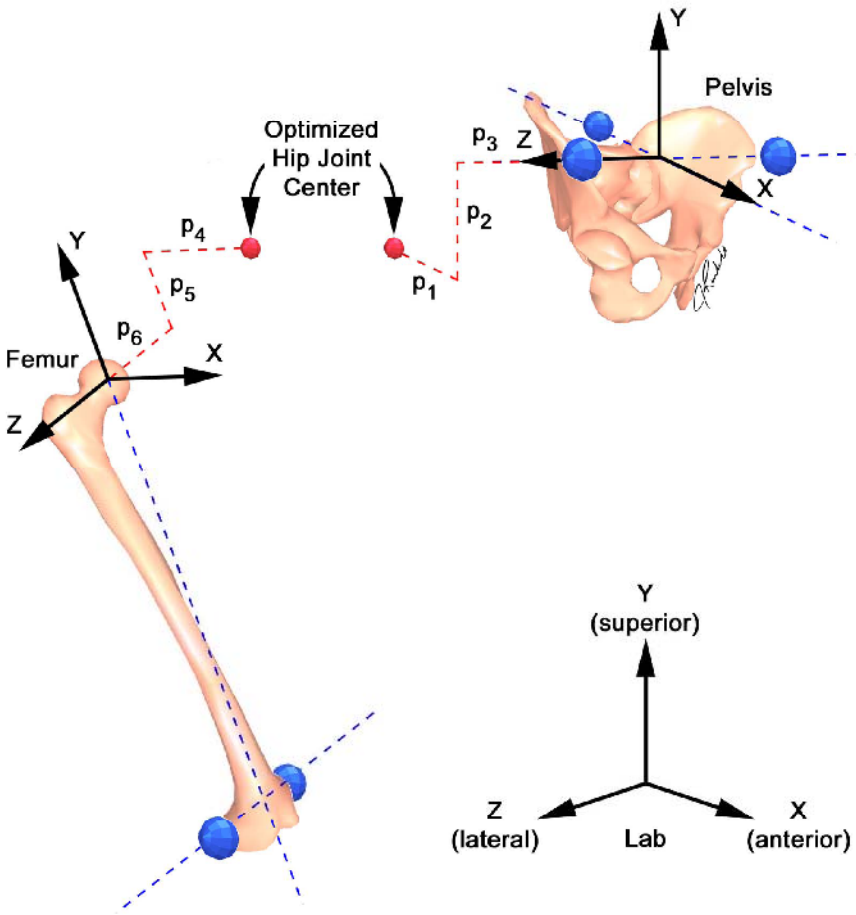

Figure 2-2. Illustration of the 3 DOF right hip joint center simultaneously defined in the pelvis and right femur segments and the 6 translational parameters optimized to determine the functional hip joint center location.

Table 2-2. Descriptions of the hip joint parameters.

Hip Joint Parameter	Description
p_1	Anterior-posterior location in pelvis segment.
p_2	Superior-inferior location in pelvis segment.
p_3	Medial-lateral location in pelvis segment.
p_4	Anterior-posterior location in femur segment.
p_5	Superior-inferior location in femur segment.
p_6	Medial-lateral location in femur segment.

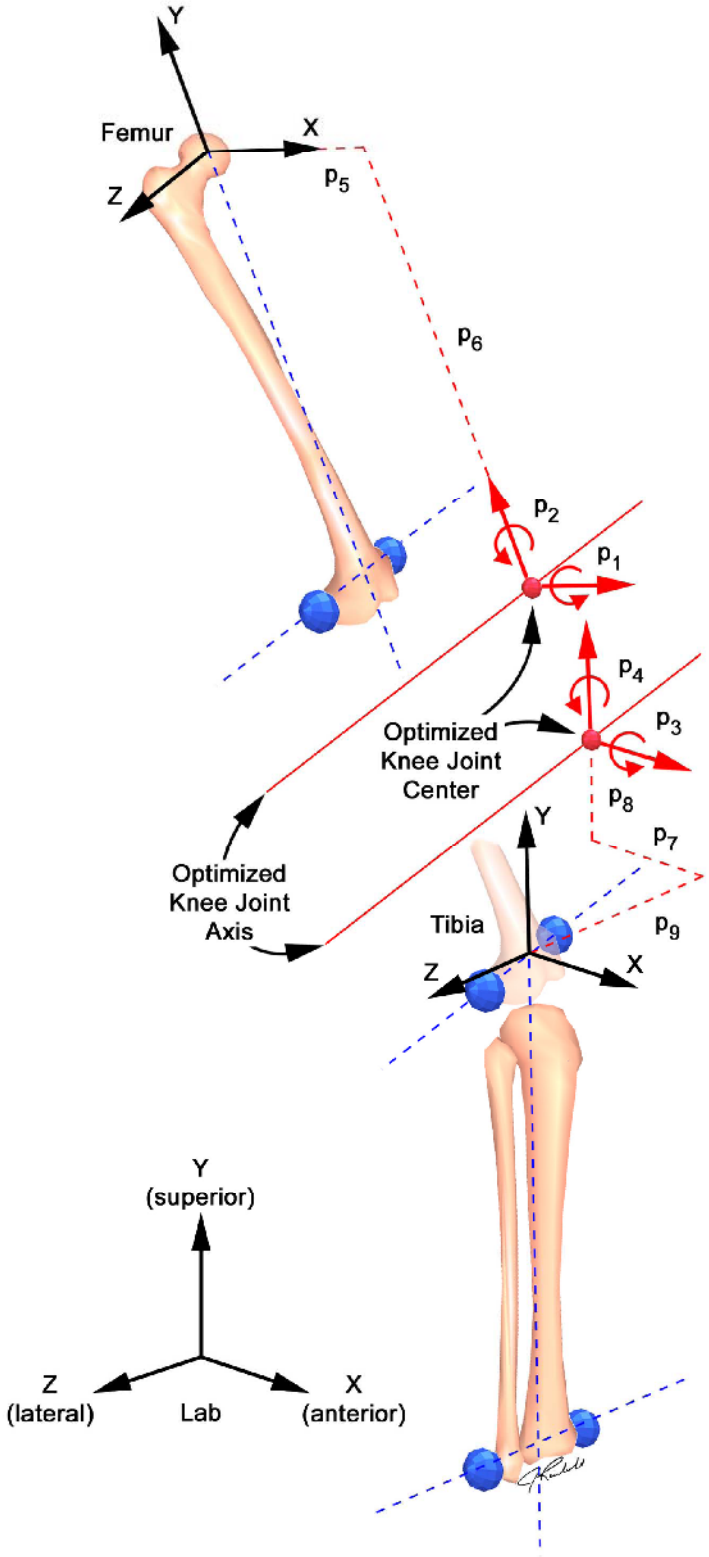

Figure 2-3. Illustration of the 1 DOF right knee joint simultaneously defined in the right femur and right tibia segments and the 4 rotational and 5 translational parameters optimized to determine the knee joint location and orientation.

Table 2-3. Descriptions of the knee joint parameters.

Knee Joint Parameter	Description
p_1	Adduction-abduction rotation in femur segment.
p_2	Internal-external rotation in femur segment.
p_3	Adduction-abduction rotation in tibia segment.
p_4	Internal-external rotation in tibia segment.
p_5	Anterior-posterior location in femur segment.
p_6	Superior-inferior location in femur segment.
p_7	Anterior-posterior location in tibia segment.
p_8	Superior-inferior location in tibia segment.
p_9	Medial-lateral location in tibia segment.

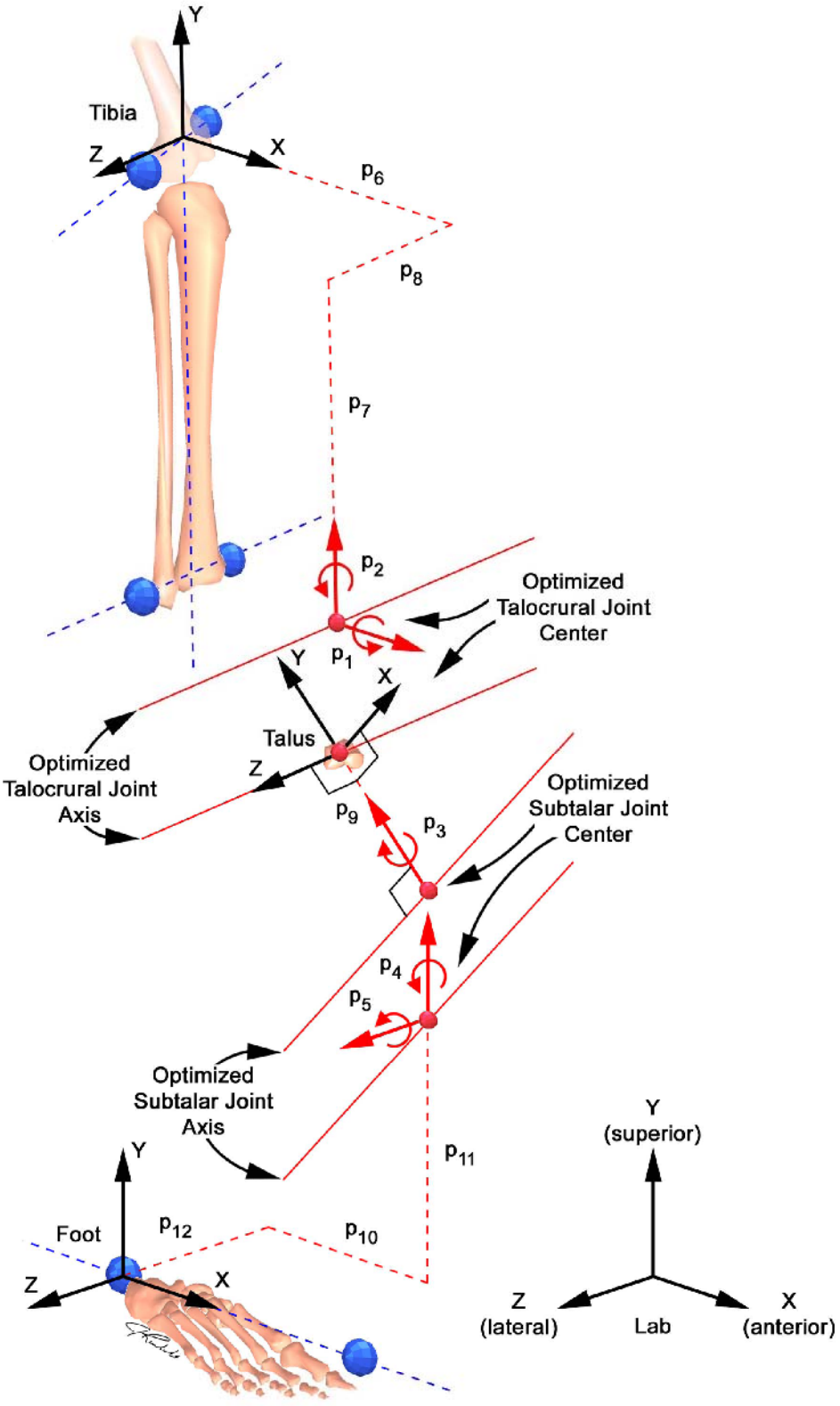

Figure 2-4. Illustration of the 2 DOF right ankle joint complex simultaneously defined in the right tibia, talus, and foot segments and the 5 rotational and 7 translational parameters optimized to determine the joint locations and orientations.

Table 2-4. Descriptions of the ankle joint parameters.

Ankle Joint Parameter	Description
p_1	Adduction-abduction rotation of talocrural in tibia segment.
p_2	Internal-external rotation of talocrural in tibia segment.
p_3	Internal-external rotation of subtalar in talus segment.
p_4	Internal-external rotation of subtalar in foot segment.
p_5	Dorsi-plantar rotation of subtalar in foot segment.
p_6	Anterior-posterior location of talocrural in tibia segment.
p_7	Superior-inferior location of talocrural in tibia segment.
p_8	Medial-lateral location of talocrural in tibia segment.
p_9	Superior-inferior location of subtalar in talus segment.
p_{10}	Anterior-posterior location of subtalar in foot segment.
p_{11}	Superior-inferior location of subtalar in foot segment.
p_{12}	Medial-lateral location of subtalar in foot segment.

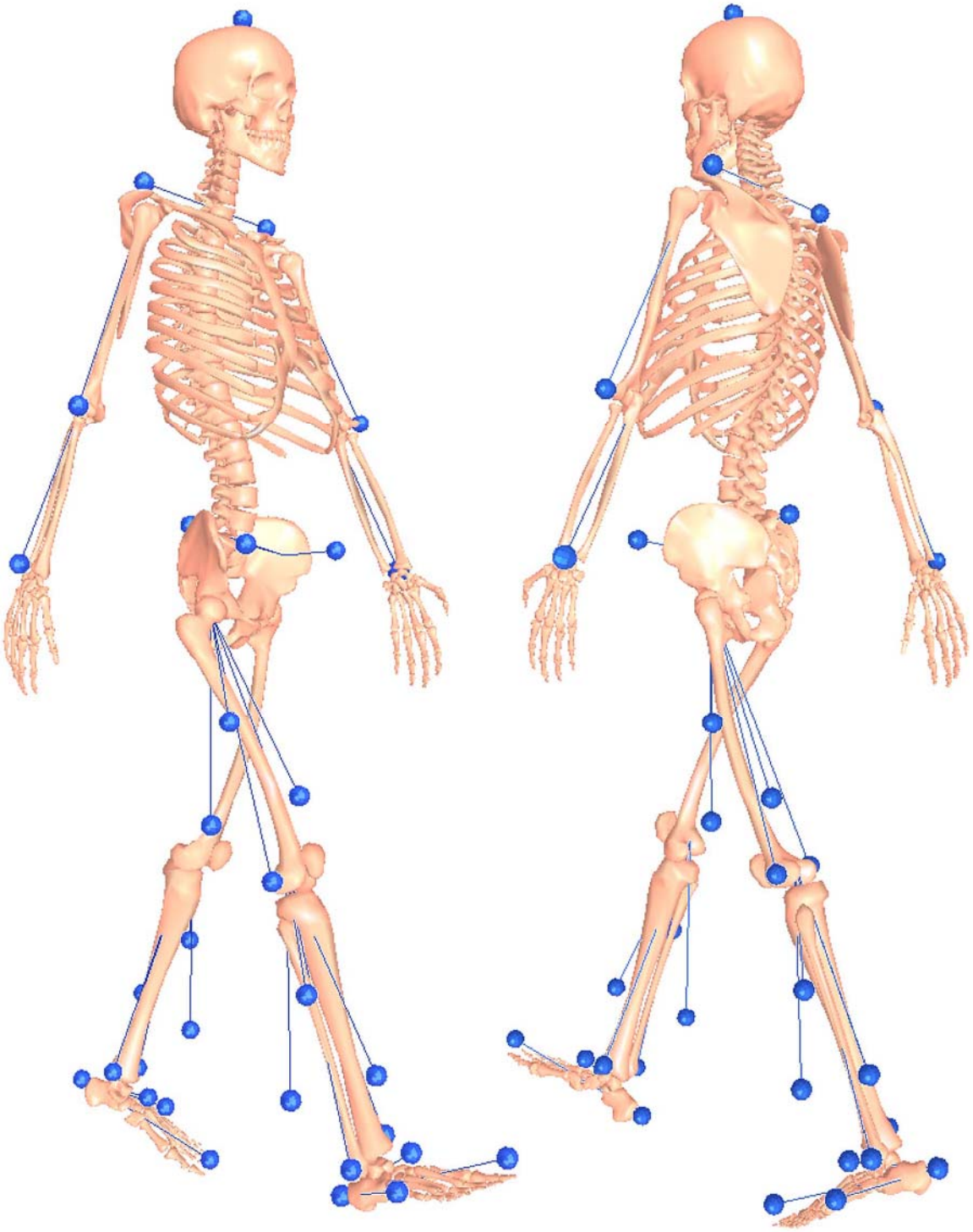

Figure 2-5. Illustration of the modified Cleveland Clinic marker set used during static and dynamic motion capture trials. Note: the background femur and knee markers have been omitted for clarity and the medial and lateral markers for the knee and ankle are removed following the static trial.

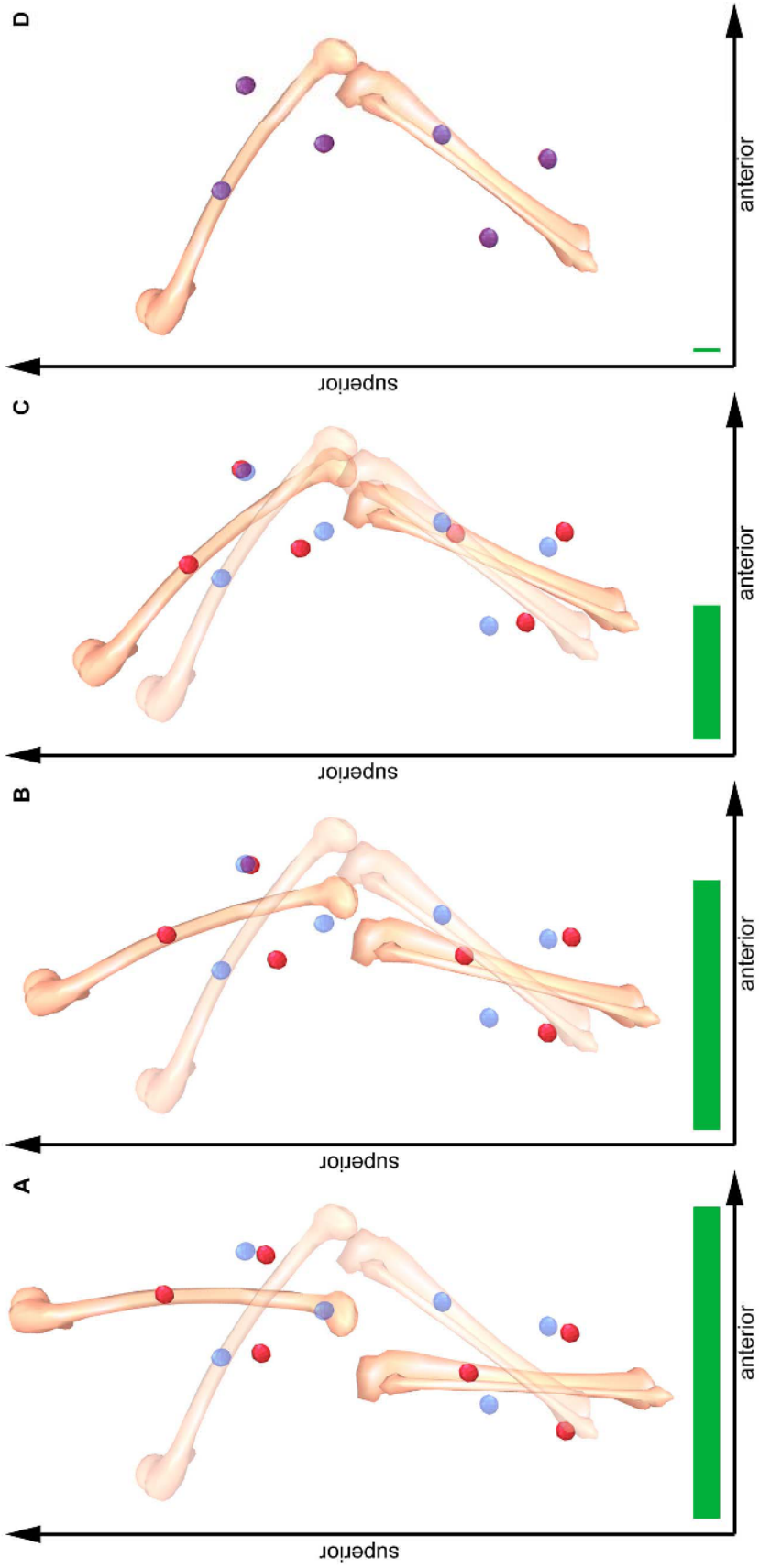

Figure 2-6. Phase one optimization convergence illustration series for the knee joint, where synthetic markers are blue, model markers are red, and root-mean-square (RMS) marker distance error is green. Given synthetic marker data without noise and a synthetic knee flexion angle = 90°, A) is the initial model knee flexion = 0° and knee joint parameters causing joint dislocation, B) is the model knee flexion = 30° and improved knee joint parameters, C) is the model knee flexion = 60° and nearly correct knee joint parameters, and D) is the final model knee flexion = 90° and ideal knee joint parameters.

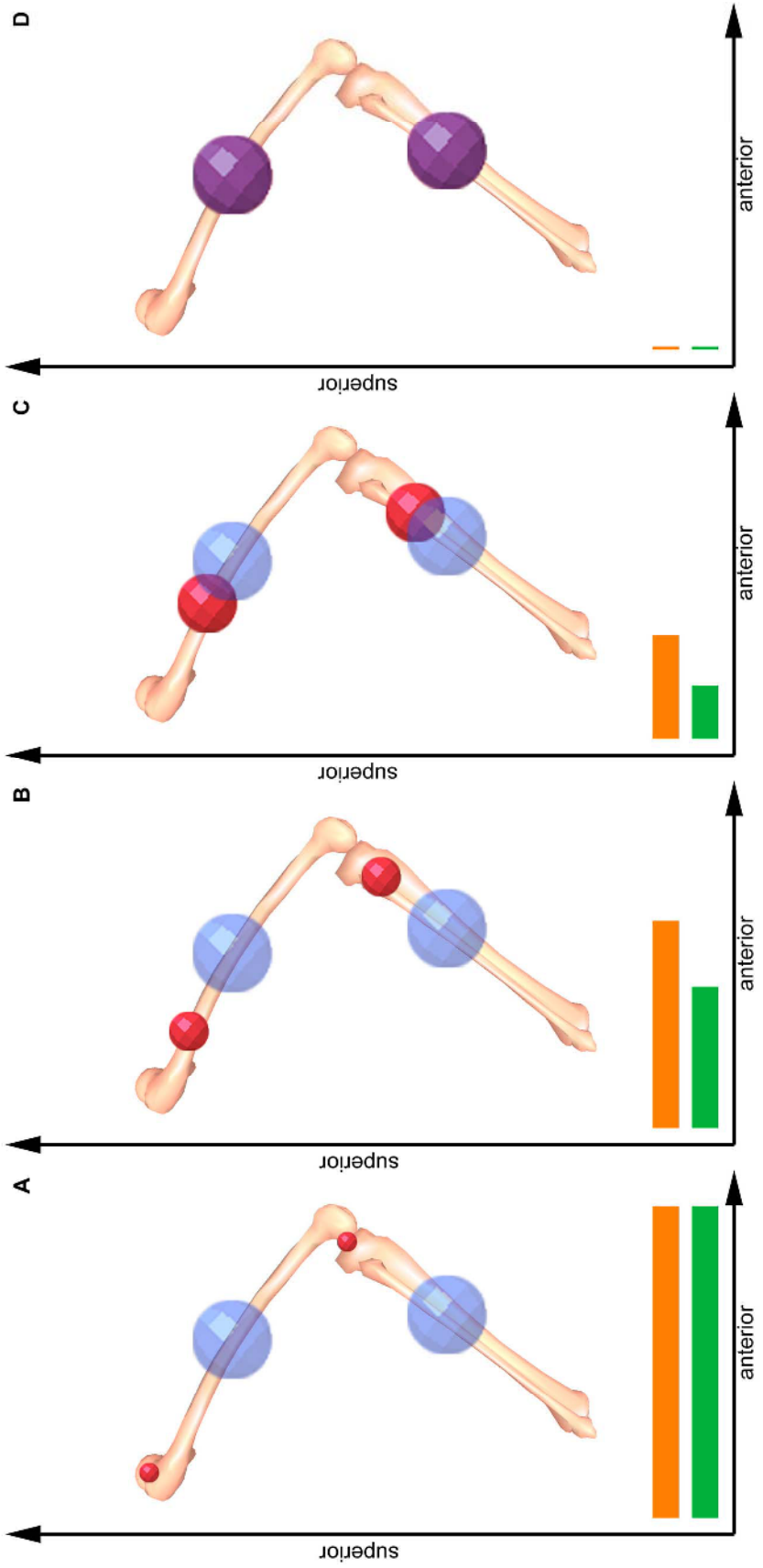

Figure 2-7. Phase two optimization convergence illustration series for the knee joint, where synthetic masses are blue, model masses are red, and root-mean-square (RMS) residual pelvis forces and torques are orange and green, respectively. Given synthetic kinetic data without noise and a synthetic knee flexion motion, A) is the initial model thigh and shank inertial parameters, B) is the improved thigh and shank inertial parameters, C) is the nearly correct thigh and shank inertial parameters, and D) is the final model thigh and shank inertial parameters.

Table 2-5. Summary of root-mean-square (RMS) joint parameter and marker distance errors produced by the phase one optimization and anatomic landmark methods for three types of movement data. Experimental data were from isolated joint and gait motions measured using a video-based motion analysis system with three surface markers per body segment. Synthetic marker data were generated by applying the experimental motions to a nominal kinematic model with and without superimposed numerical noise. The isolated joint motions were non-weight bearing and utilized larger joint excursions than did the gait motion. For the anatomical landmark method, only the optimization involving model motion was performed since the joint parameters were specified. The individual joint optimizations used isolated joint motion data while the full leg optimization used gait motion data.

Movement data	**Method**	**RMS error**	**Hip only**	**Knee only**	**Ankle only**	**Full leg**
Synthetic without Noise	Phase one optimization	Marker distances (mm)	9.82e-09	3.58e-08	1.80e-08	2.39e-06
		Orientation parameters (°)	n/a	4.68e-04	6.46e-03	5.45e-03
		Position parameters (mm)	4.85e-05	8.69e-04	6.35e-03	1.37e-02
Synthetic with Noise	Phase one optimization	Marker distances (mm)	6.62	5.89	5.43	5.49
		Orientation parameters (°)	n/a	0.09	3.37	3.43
		Position parameters (mm)	0.55	0.59	1.21	3.65
Experimental	Phase one optimization	Marker distances (mm)	3.73	1.94	1.43	4.04
	Anatomical landmarks	Marker distances (mm)	4.47	4.03	4.44	6.08

Table 2-6. Comparison of joint parameters predicted by anatomical landmark methods, phase one optimization involving individual joints separately, and phase one optimization involving all joints simultaneously. Body segment indicates the segment in which the associated joint parameter is fixed. For a graphical depiction of the listed joint parameters, consult Figure 2, Figure 3, and Figure 4.

Joint	Joint parameter	Body segment	Anatomical landmarks	Single joint optimization			Full leg optimization		
				Synthetic without noise	Synthetic with noise	Experimental	Synthetic without noise	Synthetic with noise	Experimental
Hip	Anterior position (mm)	Pelvis	-53.88	-53.88	-53.84	-32.62	-53.89	-53.35	-29.41
	Superior position (mm)	Pelvis	-83.26	-83.26	-82.76	-106.53	-83.25	-76.40	-92.15
	Lateral position (mm)	Pelvis	-78.36	-78.36	-79.30	-90.87	-78.36	-79.30	-90.87
	Anterior position (mm)	Thigh	0.00	0.00	0.49	8.88	-0.01	4.35	27.08
	Superior position (mm)	Thigh	0.00	0.00	0.47	-25.33	0.02	5.55	-11.59
	Lateral position (mm)	Thigh	0.00	0.00	-0.46	-18.13	0.00	-0.45	-18.13
Knee	Frontal plane orientation (°)	Thigh	0.00	0.00	-0.01	-4.39	0.01	-0.33	-7.59
	Transverse plane orientation (°)	Thigh	0.00	0.00	-0.09	-2.49	0.00	-1.07	-3.96
	Frontal plane orientation (°)	Shank	4.27	4.27	4.13	-0.15	4.28	3.52	-0.98
	Transverse plane orientation (°)	Shank	-17.11	-17.11	-17.14	-18.96	-17.11	-18.11	-23.34
	Anterior position (mm)	Thigh	0.00	0.00	-0.74	3.01	0.00	2.32	10.97
	Superior position (mm)	Thigh	-419.77	-419.77	-420.20	-410.44	-419.79	-425.80	-408.70
	Anterior position (mm)	Shank	0.00	0.00	-0.18	0.52	0.00	7.63	7.22
	Superior position (mm)	Shank	0.00	0.00	-0.53	2.68	-0.02	-4.49	10.13
	Lateral position (mm)	Shank	0.00	0.00	-0.84	-6.79	0.00	-1.63	2.67
Ankle (talocrural)	Frontal plane orientation (°)	Shank	-12.22	-12.21	-16.29	-11.18	-12.22	-12.81	-2.64
	Transverse plane orientation (°)	Shank	0.00	0.01	3.84	-23.89	0.00	8.79	-18.12
	Anterior position (mm)	Shank	0.00	0.01	0.24	4.14	0.00	-2.09	-3.29
	Superior position (mm)	Shank	-377.44	-377.45	-379.20	-395.73	-377.45	-379.99	-393.29
	Lateral position (mm)	Shank	0.00	-0.01	2.03	7.08	0.00	2.03	7.08
Ankle (subtalar)	Transverse plane orientation (°)	Talus	-35.56	-35.56	-40.56	-27.86	-35.56	-40.57	-27.86
	Transverse plane orientation (°)	Foot	-23.00	-23.00	-23.34	-34.79	-23.00	-23.34	-34.79
	Sagittal plane orientation (°)	Foot	42.00	42.00	42.59	31.34	42.00	42.59	31.34
	Superior position (mm)	Talus	-10.00	-10.00	-9.22	-5.77	10.00	-9.22	-5.77
	Anterior position (mm)	Foot	93.36	93.36	93.95	87.31	93.36	93.95	87.31
	Superior position (mm)	Foot	54.53	54.52	53.34	39.68	54.52	53.34	39.68
	Lateral position (mm)	Foot	-6.89	-6.89	-6.06	-3.80	-6.89	-6.06	-3.80

Table 2-7. Differences between joint parameters predicted by anatomical landmark methods and phase one optimizations. Body segment indicates the segment in which the associated joint parameter is fixed. For actual joint parameter values, consult Table 2-6. For a graphical depiction of the listed joint parameters, consult Figure 2, Figure 3, and Figure 4.

Joint	Joint parameter	Body segment	Single joint optimization		Full leg optimization	
			Synthetic difference	Experimental difference	Synthetic difference	Experimental difference
Hip	Anterior position (mm)	Pelvis	0.03	21.26	0.53	24.47
	Superior position (mm)	Pelvis	0.51	-23.27	6.86	-8.89
	Lateral position (mm)	Pelvis	-0.94	-12.51	-0.94	-12.51
	Anterior position (mm)	Thigh	0.49	8.88	4.35	27.08
	Superior position (mm)	Thigh	0.47	-25.33	5.55	-11.59
	Lateral position (mm)	Thigh	-0.46	-18.13	-0.46	-18.13
Knee	Frontal plane orientation (°)	Thigh	-0.01	-4.39	-0.33	-7.59
	Transverse plane orientation (°)	Thigh	-0.09	-2.49	-1.08	-3.96
	Frontal plane orientation (°)	Shank	-0.14	-4.42	-0.76	-5.25
	Transverse plane orientation (°)	Shank	-0.03	-1.85	-1.01	-6.23
	Anterior position (mm)	Thigh	-0.74	3.01	2.32	10.97
	Superior position (mm)	Thigh	-0.43	9.33	-6.04	11.07
	Anterior position (mm)	Shank	-0.18	0.52	7.64	7.22
	Superior position (mm)	Shank	-0.53	2.68	-4.49	10.13
	Lateral position (mm)	Shank	-0.84	-6.79	-1.63	2.67
Ankle (talocrural)	Frontal plane orientation (°)	Shank	-4.08	1.04	-0.59	9.58
	Transverse plane orientation (°)	Shank	3.85	-23.89	8.79	-18.12
	Anterior position (mm)	Shank	0.24	4.14	-2.09	-3.29
	Superior position (mm)	Shank	-1.76	-18.29	-2.54	-15.85
	Lateral position (mm)	Shank	2.03	7.08	2.03	7.08
Ankle (subtalar)	Transverse plane orientation (°)	Talus	-5.01	7.70	-5.01	7.70
	Transverse plane orientation (°)	Foot	-0.34	-11.79	-0.34	-11.79
	Sagittal plane orientation (°)	Foot	0.59	-10.66	0.59	-10.66
	Superior position (mm)	Talus	0.78	4.23	0.78	4.23
	Anterior position (mm)	Foot	0.59	-6.05	0.59	-6.05
	Superior position (mm)	Foot	-1.19	-14.85	-1.19	-14.85
	Lateral position (mm)	Foot	0.82	3.09	0.82	3.09

Table 2-8. Summary of root-mean-square (RMS) inertial parameter and pelvis residual load errors produced by the phase two optimization and anatomic landmark methods for three types of movement data. Experimental data were from a gait motion measured using a video-based motion analysis system with three surface markers per body segment. Synthetic marker data were generated by applying the experimental motion to a nominal kinematic model with and without superimposed numerical noise.

Movement data	**Method**	**RMS error**				
		Force (N)	**Torque (N*m)**	**Inertia (kg*m^2)**	**Mass (kg)**	**Center of mass (m)**
Synthetic without Noise	Phase 2 optimization	8.04e-10	2.16e-10	5.13e-13	1.22e-10	7.11e-13
Synthetic with Noise (correct seed)	Phase 2 optimization	16.92	4.93	5.67e-03	1.08	6.64e-03
Synthetic with Noise (random seeds)	Phase 2 optimization	16.96±0.44	5.24±0.23	7.45e-02±1.81e-02	1.33±0.39	2.16e-02±2.92e-03
Experimental	Phase 2 optimization	27.89	12.66	n/a	n/a	n/a
	Anatomical landmarks	34.81	13.75	n/a	n/a	n/a

Table 2-9 Comparison of inertial parameters predicted by anatomical landmark methods and phase two optimizations. Body segment indicates the segment in which the associated inertial parameter is fixed. Direction indicates the means in which the associated inertial parameter was applied.

Category	Body segment	Direction	Anatomical landmarks	Synthetic without noise	Synthetic with noise		Experimental
					Correct seed	Random seeds (10 cases)	
Mass (kg)	Pelvis	n/a	7.69	7.69	8.11	6.98±1.87	7.63
	Thigh		9.74	9.74	10.76	11.19±1.02	8.91
	Shank		2.98	2.98	3.25	3.37±0.39	2.95
	Foot		1.26	1.26	1.37	1.40±0.29	1.29
	Head & trunk		26.99	26.99	23.61	23.88±1.34	26.82
	Upper arm		1.86	1.86	1.82	1.56±0.49	1.87
	Lower arm & hand		1.53	1.53	1.63	1.75±0.47	1.53
Center of mass (m)	Pelvis	Anterior	-9.36e-02	-9.36e-02	-9.63e-02	-1.00e-01±2.29e-02	-9.33e-02
		Superior	-2.37e-02	-2.37e-02	-2.33e-02	-2.49e-02±5.44e-03	-2.37e-02
		Lateral	0.00	-2.35e-13	6.57e-13	8.06e-13±4.02e-13	6.07e-13
	Thigh	Anterior	0.00	1.54e-13	4.02e-13	7.76e-13±2.06e-13	4.86e-13
		Superior	-1.68e-01	-1.68e-01	-1.65e-01	-1.58e-01±1.84e-02	-1.59e-01
		Lateral	0.00	-1.49e-14	1.58e-12	2.41e-12±8.05e-13	8.91e-13
	Shank	Anterior	0.00	1.22e-14	-5.41e-13	-1.91e-13±6.20e-13	7.62e-13
		Superior	-1.72e-01	-1.72e-01	-1.89e-01	-1.89e-01±4.48e-02	-1.80e-01
		Lateral	0.00	6.59e-14	3.15e-13	5.65e-13±2.72e-13	4.56e-13
	Foot	Anterior	9.21e-02	9.21e-02	8.73e-02	8.17e-02±1.90e-02	9.27e-02
		Superior	-1.60e-04	-1.60e-04	-4.19e-04	-4.12e-04±1.19e-04	-1.60e-04
		Lateral	0.00	-1.81e-14	1.26e-14	9.35e-14±8.93e-14	1.85e-14
	Head & trunk	Anterior	0.00	1.92e-13	-8.33e-13	-8.96e-13±2.35e-12	8.21e-13
		Superior	-1.44e-01	-1.44e-01	-1.69e-01	-1.87e-01±1.38e-02	-1.42e-01
		Lateral	0.00	-2.56e-14	1.66e-12	2.34e-12±7.09e-13	4.45e-13
	Upper arm	Anterior	0.00	4.74e-14	-3.21e-13	-2.69e-13±2.60e-13	6.15e-13
		Superior	-1.84e-01	-1.84e-01	-1.86e-01	-1.95e-01±4.96e-02	-1.84e-01
		Lateral	0.00	-1.79e-14	3.51e-13	4.19e-13±2.45e-13	7.92e-13
	Lower arm & hand	Anterior	0.00	5.59e-14	1.45e-13	2.32e-13±3.58e-13	9.22e-13
		Superior	-1.85e-01	-1.85e-01	-1.97e-01	-1.89e-01±4.36e-02	-1.85e-01
		Lateral	0.00	-3.85-e14	2.86e-13	4.13e-13±1.59e-13	7.38e-13
Moment of inertia ($kg*m^2$)	Pelvis	Anterior	6.83e-02	6.83e-02	6.83e-02	6.60e-02±2.30e-02	6.83e-02
		Superior	6.22e-02	6.22e-02	6.21e-02	5.98e-02±1.81e-02	6.22e-02
		Lateral	5.48e-02	5.48e-02	5.47e-02	5.25e-02±1.64e-02	5.48e-02
	Thigh	Anterior	1.78e-01	1.78e-01	1.80e-01	1.67e-01±5.39e-02	1.78e-01
		Superior	3.66e-02	3.66e-02	3.65e-02	3.71e-02±1.35e-02	3.66e-02
		Lateral	1.78e-01	1.78e-01	1.74e-01	2.06e-01±5.31e-02	1.78e-01
	Shank	Anterior	2.98e-02	2.98e-02	2.97e-02	3.06e-02±1.19e-02	2.98e-02
		Superior	4.86e-03	4.86e-03	4.86e-03	4.01e-03±1.04e-03	4.86e-03
		Lateral	2.84e-02	2.84e-02	2.86e-02	2.75e-02±6.65e-03	2.84e-02
	Foot	Anterior	2.38e-03	2.38e-03	2.29e-03	2.27e-03±6.45e-04	2.38e-03
		Superior	4.56e-03	4.56e-03	4.58e-03	4.90e-03±1.29e-03	4.56e-03
		Lateral	3.08e-03	3.08e-03	2.99e-03	3.02e-03±6.57e-04	3.08e-03
	Head & trunk	Anterior	9.51e-01	9.51e-01	9.18e-01	8.96e-01±3.35e-01	9.51e-01
		Superior	2.27e-01	2.27e-01	2.27e-01	1.93e-01±3.62e-02	2.27e-01
		Lateral	8.41e-01	8.41e-01	8.37e-01	9.99e-01±2.68e-01	8.41e-01
	Upper arm	Anterior	1.53e-02	1.53e-02	1.53e-02	1.44e-02±5.65e-03	1.53e-02
		Superior	4.71e-03	4.71e-03	4.71e-03	4.57e-03±1.29e-03	4.71e-03
		Lateral	1.37e-02	1.37e-02	1.37e-02	1.56e-02±3.29e-03	1.37e-02
	Lower arm & hand	Anterior	1.97e-02	1.97e-02	1.97e-02	2.06e-02±4.97e-03	1.97e-02
		Superior	1.60e-03	1.60e-03	1.60e-03	1.41e-03±5.02e-04	1.60e-03
		Lateral	2.05e-02	2.05e-02	2.04e-02	2.41e-02±3.78e-03	2.05e-02

Table 2-10. Differences between inertial parameters predicted by anatomical landmark methods and phase two optimizations. Body segment indicates the segment in which the associated joint parameter is fixed. Direction indicates the means in which the associated inertial parameter was applied. For actual joint parameter values, consult Table 2-9.

Category	Body segment	Direction	Synthetic differences		Experimental differences
			Correct seed	Random seeds (10 cases)	
Mass (kg)	Pelvis	n/a	4.28e-01	-7.01e-01±1.87	-5.66e-02
	Thigh		1.02	1.45±1.02	-8.29e-01
	Shank		2.69e-01	3.89e-01±3.86e-01	-3.11e-02
	Foot		1.29e-01	1.62e-01±2.95e-01	3.53e-02
	Head and trunk		-3.38	-3.11±1.34	-1.75e-01
	Upper arm		-4.62e-02	-3.05e-01±4.85e-01	1.46e-03
	Lower arm and hand		1.01e-01	2.15e-01±4.67e-01	-1.89e-03
Center of mass (m)	Pelvis	Anterior	-2.69e-03	-6.51e-03±2.29e-02	2.30e-04
		Superior	4.13e-04	-1.24e-03±5.44e-03	1.12e-05
		Lateral	6.57e-13	8.06e-13±4.02e-13	6.07e-13
	Thigh	Anterior	4.02e-13	7.76e-13±2.06e-13	4.86e-13
		Superior	3.48e-03	1.01e-02±1.84e-02	9.81e-03
		Lateral	1.58e-12	2.41e-12±8.05e-13	8.91e-13
	Shank	Anterior	-5.41e-13	-1.91e-13±6.20e-13	7.62e-13
		Superior	-1.66e-02	-1.73e-02±4.48e-02	-7.65e-03
		Lateral	3.15e-13	5.65e-13±2.72e-13	4.56e-13
	Foot	Anterior	-4.83e-03	-1.04e-02±1.90e-02	6.30e-04
		Superior	-5.25e-08	7.39e-06±1.19e-04	9.50e-13
		Lateral	1.26e-14	9.35e-14±8.93e-14	1.85e-14
	Head and trunk	Anterior	-8.33e-13	-8.96e-13±2.35e-12	8.21e-13
		Superior	-2.47e-02	-4.31e-02±1.38e-02	1.66e-03
		Lateral	1.66e-12	2.34e-12±7.09e-13	4.45e-13
	Upper arm	Anterior	-3.21e-13	-2.69e-13±2.60e-13	6.15e-13
		Superior	-2.40e-03	-1.15e-02±4.96e-02	1.10e-04
		Lateral	3.51e-13	4.19e-13±2.45e-13	7.92e-13
	Lower arm and hand	Anterior	1.45e-13	2.32e-13±3.58e-13	9.22e-13
		Superior	-1.29e-02	-4.21e-03±4.36e-02	3.70e-04
		Lateral	2.86e-13	4.13e-13±1.59e-13	7.38e-13
Moment of inertia ($kg*m^2$)	Pelvis	Anterior	5.53e-05	-2.24e-03±2.30e-02	1.95e-04
		Superior	-1.11e-04	-2.41e-03±1.81e-02	-9.03e-04
		Lateral	-1.21e-04	-2.28e-03±1.64e-02	-1.19e-05
	Thigh	Anterior	2.06e-03	-1.14e-02±5.39e-02	2.86e-03
		Superior	-7.14e-05	5.67e-04±1.35e-02	-1.45e-04
		Lateral	-4.56e-03	2.73e-02±5.31e-02	-9.06e-03
	Shank	Anterior	-9.91e-05	8.51e-04±1.19e-02	-5.98e-04
		Superior	6.80e-07	-8.49e-04±1.04e-03	1.85e-06
		Lateral	2.09e-04	-9.19e-04±6.65e-03	4.15e-04
	Foot	Anterior	-5.94e-07	-1.73e-05±6.45e-04	-9.07e-08
		Superior	-8.59e-08	3.16e-04±1.29e-03	-6.41e-07
		Lateral	3.06e-06	2.87e-05±6.57e-04	1.36e-05
	Head and trunk	Anterior	-3.30e-02	-5.56e-02±3.35e-01	-3.08e-02
		Superior	-6.15e-04	-3.37e-02±3.62e-02	-2.87e-03
		Lateral	-4.13e-03	1.59e-01±2.68e-01	-1.73e-02
	Upper arm	Anterior	-1.62e-05	-9.11e-04±5.65e-03	-1.37e-04
		Superior	-1.79e-07	-4.14e-05±1.29e-03	-9.40e-07
		Lateral	-7.90e-07	1.97e-03±3.29e-03	-1.60e-06
	Lower arm and hand	Anterior	-1.63e-05	8.91e-04±4.97e-03	-1.09e-04
		Superior	-8.95e-08	-1.95e-04±5.02e-04	-7.50e-07
		Lateral	-5.84e-05	3.59e-03±3.78e-03	-1.15e-05

CHAPTER 3
EFFECT OF MODEL PARAMETER VARIATIONS ON INVERSE DYNAMICS RESULTS USING MONTE CARLO SIMULATIONS

Background

"One of the most valuable biomechanical variables to have for the assessment of any human movement is the time history of the moments of force at each joint" (Winter, 1980). There are countless applications involving the investigation of human movement ranging from sports medicine to pathological gait. In all cases, the moment of force, or torque, at a particular joint is a result of several factors: muscle forces, muscle moment arms, ligament forces, contact forces due to articular surface geometry, positions and orientations of axes of rotation, and inertial properties of body segments. A common simplification is muscles generate the entire joint torque by assuming ligament forces are insignificant and articular contact forces act through a chosen joint center (Challis and Kerwin, 1996). Individual muscle forces are estimated from resultant joint torques often computed by inverse dynamics analyses. In the end, inverse dynamics computations depend upon chosen model parameters, namely positions and orientations of joint axes parameters (JPs) and inertial property parameters (IPs) of body segments.

The literature contains a variety of methods investigating the sensitivity of inverse dynamics torques to JPs and IPs. Two elbow joint torques were analyzed during a maximal speed dumbbell curl motion as one or more parameters were changed by the corresponding estimated uncertainty value up to 10mm for joint centers and 10% for inertial properties (Challis and Kerwin, 1996). The knee flexion-extension torque has

been studied for multiple walking speeds while changing the knee center location by ±10mm in the anterior-posterior direction (Holden and Stanhope, 1998). Hip forces and torques have been examined for gait as planar leg inertial properties were individually varied over nine steps within ±40% (Pearsall and Costigan, 1999). Knee forces and torques were evaluated for a planar harmonic oscillating motion as inertial properties varied by ±5% (Andrews and Mish, 1996). Directly related to knee joint torque, knee kinematics were investigated during gait when the rotation axes varied by ±10° (Croce *et al.*, 1996).

This study performs a series of Monte Carlo analyses relating to inverse dynamics using instantiations of a three-dimensional (3D) full-body gait model with isolated and simultaneous variations of JP and IP values. In addition, noise parameter (NP) variations representing kinematic noise were implemented separately. Uniform distribution of each parameter was chosen within bounds consistent with previous studies. Subsequently, kinematics were identified by optimizing the fitness of the model motion to the experimental motion. The number of instantiations was sufficient for convergence of inverse dynamics torque values.

Methods

Experimental kinematic and kinetic gait data were collected from a single subject using a video-based motion analysis system (Motion Analysis Corporation, Santa Rosa, CA) and two force plates (AMTI, Watertown, MA). Institutional review board approval and informed consent were obtained prior to the experiments.

A parametric 3D, 27 degree-of-freedom (DOF), full-body gait model (Figure 2-1, Table 2-1) was constructed, whose equations of motion were derived with the symbolic manipulation software, Autolev™ (OnLine Dynamics, Sunnyvale, CA). The pelvis was

connected to ground via a 6 DOF joint and the remaining 13 segments comprised four open chains branching from the pelvis. The positions and orientations of joint axes within adjacent segment coordinate systems were defined by unique JPs. The segment masses, mass centers, and moments of inertia were described by unique IPs. Anatomic landmark methods were used to estimate nominal values for 84 IPs (de Leva, 1996) and 98 JPs (Bell *et al.*, 1990, Churchill *et al.*, 1998, Inman, 1976). Select model parameters were identified via optimization as described previously in Chapter 2 (Reinbolt and Fregly, 2005).

A series of Monte Carlo analyses relating to inverse dynamics were performed using instantiations the full-body gait model with isolated and simultaneous variations of JP and IP values within 25%, 50%, 75%, and 100% of the associated maximum. Uniform distribution of each parameter was chosen within bounds consistent with previous studies. Joint center locations were bounded by a maximum of ±10mm (Challis and Kerwin, 1996, Holden and Stanhope, 1998). Joint axes orientations were bounded by a maximum of ±10° (Croce *et al.*, 1996). Inertial properties were bounded by a maximum of ±10% of their original values (Andrews and Mish, 1996, Challis and Kerwin, 1996, Pearsall and Costigan, 1999). New kinematics were identified by optimizing the fitness of the model motion to the experimental motion similar to Chapter 2 (Reinbolt *et al.*, 2005). The number of instantiations (e.g., 5000) was sufficient for convergence of inverse dynamics torque values. The mean and coefficient of variance (100*SD/mean) of all joint torques were within 2% of the final mean and coefficient of variance, respectively, for the last 10% of instantiations (Fishman, 1996, Valero-Cuevas *et al.*, 2003).

A separate set of Monte Carlo inverse dynamics analyses were performed with variations of NP values within 25%, 50%, 75%, and 100% of the maximum. The NP represent the amplitude of simulated skin movement artifacts. The relative movement between skin and underlying bone occurs in a continuous rather than a random fashion (Cappozzo *et al.*, 1993). Comparable to the simulated skin movement artifacts of Lu and O'Connor (1999), a continuous noise model of the form $A\sin(\omega t + \varphi)$ was used with the following uniform random parameter values: amplitude ($0 \le A \le 1$ cm), frequency ($0 \le \omega \le 25$ rad/s), and phase angle ($0 \le \varphi \le 2\pi$) (Chèze *et al.*, 1995). Noise was separately generated for each 3D coordinate of the marker trajectories.

Similar to the lower-body focus of Chapter 2, the distributions from each Monte Carlo analysis were compared for the left leg joint torque errors and marker distance errors (e.g., difference between model markers for the inverse dynamics simulation and true synthetic data cases).

Results

The distributions of mean inverse dynamics results are best summarized using a boxplot presenting five sample statistics: the minimum (or 10th percentile), the lower quartile (or 25th percentile), the median (or 50th percentile), the upper quartile (or 75th percentile) and the maximum (or 90th percentile) (Figure 3-1).

RMS and mean hip torque errors were computed in the flexion-extension, abduction-adduction, and internal-external rotation directions (Figure 3-2, Figure 3-3). Mostly due to JPs, the hip flexion-extension and abduction-adduction torques showed more variation than the internal-external rotation torque. The IPs had insignificant effect on range of hip torques. The NPs had slightly larger effects compared to IPs. The

distributions of torques were reduced by attenuating the model fitness based on percentages of parameter bounds.

RMS and mean knee torque errors were computed in the flexion-extension and abduction-adduction directions (Figure 3-2, Figure 3-3). Similar to the corresponding hip directions, the knee torques have larger spans for the abduction-adduction direction compared to the flexion-extension direction. The NPs had slightly larger effects compared to IPs. The JPs had much more effect on knee torques compared to the IPs. For the IPs case, the flexion-extension torque varied slightly more than the abduction-adduction torque. The breadth of knee torques decreased with attenuated percentages of parameter bounds.

RMS and mean ankle torque errors were computed in the plantarflexion-dorsiflexion and inversion-eversion directions (Figure 3-2, Figure 3-3). The inversion-eversion torque displayed a broader distribution compared to the plantarflexions-dorsiflexion torque. The IPs had much less effect on ankle torque distributions compared to JPs. The NPs had slightly larger effects compared to IPs. The attenuated percentages of parameter bounds condensed the spread for both torques.

RMS and mean marker distance errors were computed between the inverse dynamics simulation and synthetic data (Figure 3-2, Figure 3-3). The IPs showed marker distance errors equal to zero since true kinematics were used as inputs. The NPs represented marker distance errors consistent with the chosen numerical noise model. The JPs had the largest effect on marker distance error distributions.

Discussion

This study examined the distribution of inverse dynamics torques for a 3D full-body gait model using a series of Monte Carlo analyses simultaneously varying JPs

and IPs. It is well established that joint torque data is one of the most valuable quantities for the biomechanical investigation of human movement. As evident in the literature, investigators are concerned with the sensitivity of inverse dynamics results to uncertainties in JPs and IPs (Challis and Kerwin, 1996, Holden and Stanhope, 1998, Pearsall and Costigan, 1999, Andrews and Mish, 1996, Croce *et al.*, 1996). Assuming parameter independence and adjusting a single parameter at a time may underestimate the resulting effect of the parameter variation. Specifically concerning IPs, adjusting one type of segment parameter may change the other two types. Similar to all Monte Carlo analyses assuming parameter independence, the resulting distributions may in fact be overestimated. A more diverse assortment of full-body models are being simulated by not explicitly requiring particular body segment geometries. Nevertheless, implementing an optimization approach to maximize the fitness of the model to the experiment through determination of patient-specific JPs and IPs reduces the uncertainty of inverse dynamics results.

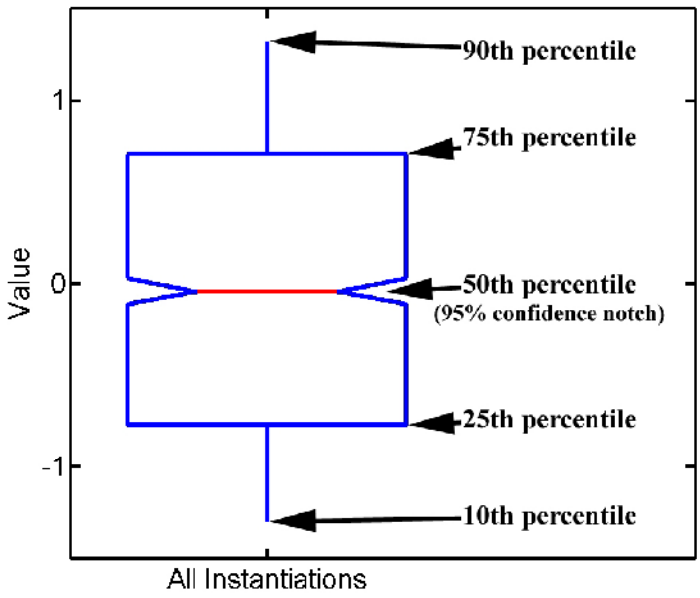

Figure 3-1. Legend of five sample statistics presented by the chosen boxplot convention.

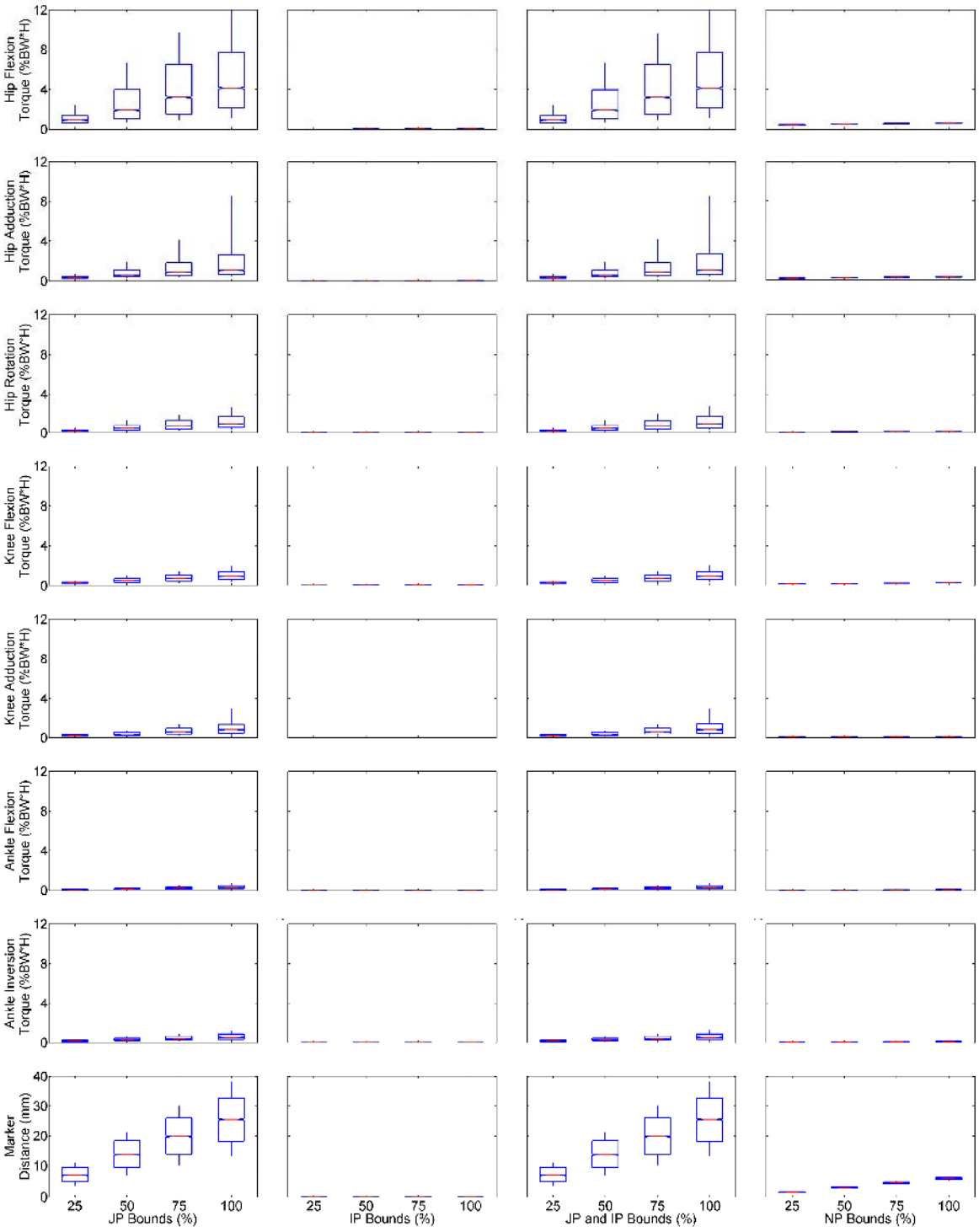

Figure 3-2. Comparison of root-mean-square (RMS) leg joint torques and marker distance error distributions. First column contains distributions from varying only joint parameters (JP). Second column contains distributions from varying only inertial parameters (IP). Third column contains distributions from varying both JPs and IPs. Fourth column contains distributions from vary only the noise amplitude parameter (NP).

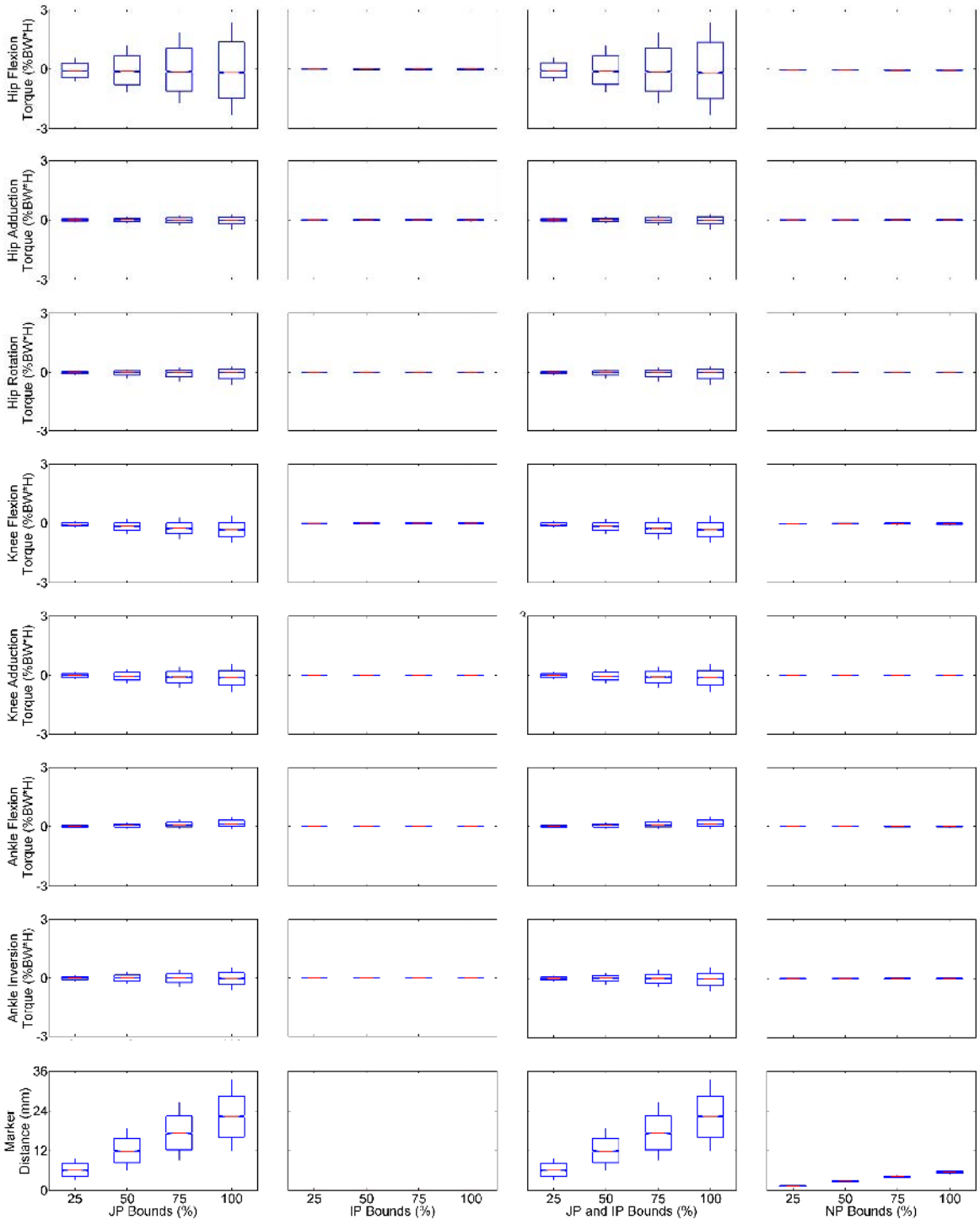

Figure 3-3. Comparison of mean leg joint torques and marker distance error distributions. First column contains distributions from varying only joint parameters (JP). Second column contains distributions from varying only inertial parameters (IP). Third column contains distributions from varying both JPs and IPs. Fourth column contains distributions from vary only the noise amplitude parameter (NP).

CHAPTER 4
BENEFIT OF AUTOMATIC DIFFERENTIATION FOR BIOMECHANICAL OPTIMIZATIONS

Background

Optimization algorithms are often used to solve biomechanical system identification or movement prediction problems employing complicated three-dimensional (3D) musculoskeletal models (Pandy, 2001). When gradient-based methods are used to solve large-scale problems involving hundreds of design variables, the computational cost of performing repeated simulations to calculate finite difference gradients can be extremely high. In addition, as 3D movement model complexity increases, there is a considerable increase in the computational expense of repeated simulations. Frequently, in spite of advances in processor performance, optimizations remain limited by computation time.

Both speed and robustness of gradient-based optimizations are dramatically improved by using an analytical Jacobian matrix (all first-order derivatives of dependent objective function variables with respect to independent design variables) rather than relying on finite difference approximations. The objective function may involve thousands or perhaps millions of lines of computer code, so the task of computing analytical derivatives by hand or even symbolically may prove impractical. For more than eight years, the Network Enabled Optimization Server (NEOS) at Argonne National Laboratory has been using Automatic Differentiation (AD), also called Algorithmic Differentiation, to compute Jacobians of remotely supplied user code (Griewank, 2000).

AD is a technique for computing derivatives of arbitrarily complex computer programs by mechanical application of the chain rule of differential calculus. AD exploits the fact every computer program, no matter how complicated, executes a sequence of elementary arithmetic operations. By applying the chain rule repeatedly to these operations, derivatives can be computed automatically and accurately to working precision.

This study evaluates the benefit of using AD methods to calculate analytical Jacobians for biomechanical optimization problems. For this purpose, a freely-available AD package, Automatic Differentiation by OverLoading in C++ (ADOL-C) (Griewank *et al.*, 1996), was applied to two biomechanical optimization problems. The first is a system identification problem for a 3D kinematic ankle joint model involving 252 design variables and 1800 objective function elements. The second is a movement prediction problem for a 3D full-body gait model involving 660 design variables and 4100 objective function elements. Both problems are solved using a nonlinear least squares optimization algorithm.

Methods

Experimental kinematic and kinetic data were collected from a single subject using a video-based motion analysis system (Motion Analysis Corporation, Santa Rosa, CA) and two force plates (AMTI, Watertown, MA). Institutional review board approval and informed consent were obtained prior to the experiments.

The ankle joint problem was first solved without AD using the Matlab (The Mathworks, Inc., Natick, MA) nonlinear least squares optimizer as in Chapter 2 (Reinbolt and Fregly, 2005). The optimization approach simultaneously adjusted joint parameter values and model motion to minimize errors between model and experimental marker

locations. The ankle joint model possessed 12 joint parameters and 12 degrees-of-freedom. Each of the 12 generalized coordinate curves was parameterized using 20 B-spline nodal points (240 total). Altogether, there were 252 design variables. The problem contained 18 error quantities for each of the 100 time frames of data. The Jacobian matrix consisted of 1800 rows and 252 columns estimated by finite difference approximations.

The movement prediction problem was first solved without AD using the same Matlab nonlinear least squares optimizer (Fregly *et al.*, 2005). The optimization approach simultaneously adjusted model motion and ground reactions to minimize knee adduction torque and 5 categories of tracking errors (foot path, center of pressure, trunk orientation, joint torque, and fictitious ground-to-pelvis residual reactions) between model and experiment. The movement prediction model possessed 27 degrees-of-freedom (21 adjusted by B-spline curves and 6 prescribed for arm motion) and 12 ground reactions. Each adjustable generalized coordinate and reaction curve was parameterized using 20 B-spline nodal points (660 total design variables). The problem contained 41 error quantities for each of the 100 time frames of data. The Jacobian matrix consisted of 4100 rows and 660 columns estimated by finite difference approximations.

ADOL-C was incorporated into each objective function to compute an analytical Jacobian matrix. This package was chosen because the objective functions were comprised of Matlab mex-files, which are dynamic link libraries of compiled C or C++ code. ADOL-C was implemented into the C++ source code by the following steps:

1. Mark the beginning and end of active section (portion computing dependent variables from independent variables) using built-in functions `trace_on` and `trace_off`, respectively.

2. Select a set of active variables (those considered differentiable at some point in the program execution) and change type from double to built-in type `adouble`.

3. Define a set of independent variables using the output stream operator (<<=).

4. Define a set of dependent variables using the input stream operator (>>=).

5. Call the built-in driver function `jacobian` to compute first-order derivatives using reverse mode AD.

6. Compile the code including built-in header file `adolc.h` and linking with built-in library file `adolc.lib`.

All optimizations with and without AD were performed on a 1.73 GHz Pentium M laptop with 2.00 GB of RAM. The computation time performance was compared.

Results

For each problem, performance comparisons of optimizing with and without AD are summarized in Table 4-1 and Table 4-2. The use of AD increased the computation time per objective function evaluation. However, the number of function evaluations necessary per optimization iteration was far less with AD. For the system identification problem, the computation time required per optimization iteration with AD was approximately 20.5% (or reduced by a factor of 4.88) of the time required without AD. For the movement prediction problem, the computation time required per optimization iteration with AD was approximately 51.1% (or reduced by a factor of 1.96) of the time required without AD. Although computation times varied with and without AD, the optimization results remained virtually identical.

Discussion

The main motivation for investigating the use of AD for biomechanical optimizations was to improve computational speed of obtaining solutions. Speed improvement for the movement prediction optimization in particular was not as significant as anticipated. Further investigation is necessary to determine the effect of AD characteristics such as forward mode vs. reverse mode and source code transformation vs. operator overloading on computational speed. Whichever AD method is used, having analytical derivatives eliminates inaccurate search directions and sensitivity to design variable scaling which can plague optimizations that use finite difference gradients. If central (more accurate) instead of forward differencing was used in the movement prediction optimization without AD, the performance improvement would have been a factor of four instead of two.

Special dynamics formulations can also be utilized to compute analytical derivatives concurrently while evaluating the equations of motion, and the trade-offs between those approaches and AD require further investigation. While AD-based analytical derivatives may be less efficient computationally than those derived using special dynamics formulations, AD provides effortless updating of the derivative calculations should the biomechanical model used in the optimization be changed.

For large-scale problems, AD provides a relatively simple means for computing analytical derivatives to improve the speed of biomechanical optimizations.

Table 4-1. Performance results for system identification problem for a 3D kinematic ankle joint model involving 252 design variables and 1800 objective function elements.

Performance Criteria	Without AD	With AD
Time per Function Evaluation (s)	0.0189	0.978
Number of Function Evaluations per Optimization Iteration	252	1
Time per Optimization Iteration (s)	4.77	0.978

Table 4-2. Performance results for movement prediction problem for a 3D full-body gait model involving 660 design variables and 4100 objective function elements.

Performance Criteria	Without AD	With AD
Time per Function Evaluation (s)	0.217	73.1
Number of Function Evaluations per Optimization Iteration	660	1
Time per Optimization Iteration (s)	143	73.1

CHAPTER 5
APPLICATION OF PATIENT-SPECIFIC DYNAMIC MODELS TO PREDICT FUNCTIONAL OUTCOMES

Background

Imagine the benefit to the healthcare provider and, more importantly, the patient, if certain clinical parameters may be evaluated pre-treatment in order to predict the post-treatment outcome. For example, a patient-specific dynamic model may be useful for planning intended surgical parameters and predicting the outcome of HTO. Researchers have identified the peak external knee adduction torque as an indicator of clinical outcome while investigating the gait of HTO patients (Andriacchi, 1994; Bryan *et al.*, 1997; Hurwitz *et al.*, 1998; Prodromos *et al.*, 1985; Wang *et al.*, 1990). Currently, no movement simulations (or other methods for that matter) allow surgeons to choose HTO surgical parameters to achieve a chosen post-surgery knee adduction torque.

There are a few gait studies evaluating effects of kinematic changes on the knee adduction torque. One study examined the effects of increased foot progression angle, or toeout gait, on minimizing knee adduction torque during walking, stair ascent, and stair descent (Manal and Guo, 2005). Another study investigated the minimization of knee adduction torque by changing lower-body kinematics without changing foot path during gait (Fregly *et al.*, 2005). No computational framework is available to perform a virtual HTO surgery and predict the resulting knee adduction torque.

This study presents the development and application of an inverse dynamics optimization approach to predict novel patient-specific gait motions, such as gait

following HTO surgery and the resulting internal knee abduction torque. To further tailor the kinematic and kinetic model developed in Chapter 2, response surface (RS) methods are used to determine weights for a cost function specific to the patient and movement task, comprising phase three of the optimization procedure. Other biomechanical studies (Chang *et al.*, 1999, Hong *et al.*, 2001) have used RS optimization methods, but this study is the first to perform inverse dynamic optimizations of gait. To increase the speed and robustness of optimizations, automatic differentiation (AD) is used to compute analytic derivatives of the inverse dynamics optimization objective function.

Methods

Experimental kinematic and kinetic gait data were collected from a single subject using a video-based motion analysis system (Motion Analysis Corporation, Santa Rosa, CA) and two force plates (AMTI, Watertown, MA). Institutional review board approval and informed consent were obtained prior to the experiments. Normal gait data was recorded to calibrate the patient-specific model parameters as described in Chapter 2. Toeout, or increased foot progression angle, gait data was gathered to calibrate the patient-specific control parameters. Wide stance gait data was collected to evaluate the calibrated model.

A parametric 3D, 27 degree-of-freedom (DOF), full-body gait model (Figure 2-1, Table 2-1) was constructed, whose equations of motion were derived with the symbolic manipulation software, Autolev™ (OnLine Dynamics, Sunnyvale, CA). The pelvis was connected to ground via a 6 DOF joint and the remaining 13 segments comprised four open chains branching from the pelvis. Anatomic landmark methods were used to estimate nominal values for 84 inertial parameters (de Leva, 1996) and 98 joint parameters (Bell *et al.*, 1990, Churchill *et al.*, 1998, Inman, 1976). Select model

parameters were identified via optimization as described previously in Chapter 2 (Reinbolt and Fregly, 2005).

The inverse dynamics optimization procedure adjusted model motion and ground reactions to minimize errors between model and experimental, or prescribed, quantities to be tracked (Equation 5-1). Specifically, the design variables were 660 B-spline nodes ($\boldsymbol{q}$, $\boldsymbol{r}$) parameterizing the generalized coordinate (q's) trajectories and ground reaction (r's) data (20 nodes per curve). The initial value for each B-spline node was chosen to be the corresponding value from normal gait. The inverse dynamics optimization cost function ($e_{predict\ outcome}$) minimized the weighted (Equation 5-2, Equation 5-3, Table 5-1) tracking errors summed over the number of time frames (nf) for the following quantities: 6 DOFs for each prescribed foot path (q_{foot}), 2 transverse plane translations for pelvis (q_{pelvis}), 3 DOFs for trunk orientation (q_{trunk}), 2 transverse plane translations for center of pressure for each foot (CoP_{foot}), 3 residual pelvis forces (F_{pelvis}), 3 residual pelvis torques (T_{pelvis}), and leg joint torques (T_{leg}). The inverse dynamics optimizations were performed with Matlab's nonlinear least squares algorithm (The Mathworks, Natick, MA) using analytical Jacobians computed by AD.

$$e_{\substack{predict\\outcome}} = \min_{\boldsymbol{q},\boldsymbol{r}} \sum_{i=1}^{nf} \left\{ \begin{array}{l} w_1 \sum_{j=1}^{2}\sum_{k=1}^{6} (\Delta q^2_{foot})_{ijk} + w_2 \sum_{j=1}^{2} (\Delta q^2_{pelvis})_{ij} + w_3 \sum_{j=1}^{3} (\Delta q^2_{trunk})_{ij} + \\ \quad w_4 \sum_{j=1}^{2}\sum_{k=1}^{2} (\Delta CoP^2_{foot})_{ijk} + w_5 \sum_{j=1}^{3} (\Delta F^2_{pelvis} + \Delta T^2_{pelvis})_{ij} + \\ \quad \sum_{j=1}^{6}\sum_{k=1}^{2} \left[\Delta T_{leg}(\boldsymbol{p}_{CP})^2\right]_{ijk} \end{array} \right\} \quad (5\text{-}1)$$

$$\boldsymbol{p}_{CP} = \begin{bmatrix} w_6 & w_7 & w_8 & w_9 & w_{10} & w_{11} \end{bmatrix} \quad (5\text{-}2)$$

$$\Delta T_{leg}(\boldsymbol{p}_{CP}) = w_6 \Delta T_{\substack{hip \\ flexion}} + w_7 \Delta T_{\substack{hip \\ adduction}} + w_8 \Delta T_{\substack{hip \\ rotation}} + w_9 \Delta T_{\substack{knee \\ flexion}} + w_{10} \Delta T_{\substack{talocrural \\ dorsiflexion}} + w_{11} \Delta T_{\substack{subtalar \\ inversion}} \quad (5\text{-}3)$$

Before predicting outcomes with the inverse dynamics optimization, the phase 3 optimization calibrated the 6 control parameters, or $w_6 - w_{11}$ (Equation 5-2, Equation 5-3, Table 5-1), to the patient's toe out gait motion. Each prescribed foot path was the only tracked quantity which was not experimentally measured beforehand. For 3 DOFs, fixed offsets (Table 5-2) were defined to approximate the predicted toeout foot path without using the exact foot path. All other tracked quantities involved the experimentally measured normal gait motion. A computationally efficient optimization was developed using RS methods to determine how well the simulated knee abduction torque matched the experimental knee abduction torque for toeout gait. Response surfaces were developed to approximate the knee abduction torque predicted by the model for various control parameter weights. A separate quadratic RS was created for each time frame of torque data (125 response surfaces) predicted by the model where the 6 control parameter weights were treated as design variables. Although separate response surface were constructed, the correlation coefficients between them was not computed. Each quadratic RS required solution of 28 unknown polynomial coefficients. A Hammersley Quasirandom Sequence was used to generate 64 sampled data points within the bounds of 0 to 10 for the 6–dimensional space. The RS coefficients were then determined via a linear least squares fit in Matlab (The Mathworks, Natick, MA). Using the response surfaces as surrogates for repeated inverse dynamic optimizations, an optimization problem was formulated to minimize errors between model predicted knee abduction torque and experimentally realized abduction torque for toeout gait. A Hammersley

Quasirandom Sequence was used to generate 1000 initial seed points within the bounds of 0 to 10 for the 6–dimensional space. The 6 control parameters resulting in the lowest cost function value were used. The kinematic and kinetic changes for the left leg were compared.

The calibrated model was evaluated by predicting wide stance gait. Similar to toeout gait, fixed offsets (Table 5-2) were defined for 3 DOFs to approximate the predicted wide stance foot path without using the exact foot path. Again, all other tracked quantities involved the experimentally measured normal gait motion. The kinematic and kinetic changes for the left leg were compared.

The calibrated model was applied to predict the outcome of HTO surgery. All tracked quantities involved the experimentally measured normal gait motion, including the prescribed foot path (e.g., all foot path offsets equaled zero). The virtual HTO surgery was performed as a lateral opening wedge osteotomy. The anterior-posterior axis of rotation was located 10 cm inferior and 5 cm lateral to the midpoint of the transepicondylar axis. The sensitivity of the knee abduction torque to the extent, or wedge angle, of the virtual HTO surgery was illustrated in for 3°, 5°, and 7°.

To demonstrate the effects of prior calibrating optimizations which determined joint parameters (phase one from Chapter 2) and inertial parameters (phase two from Chapter 2), the entire process of creation and application of patient-specific dynamic models was repeated for three additional cases: 1) phase three only (or without phase one or two), 2) phases one and three, and 3) phases two and three. The intermediate calibration and final evaluation effects on knee abduction torque results were compared.

Results

Using the response surfaces as surrogates for repeated inverse dynamic optimizations using the model calibrated with phases one, two, and three, the optimization determined control parameters (Table 5-3) that minimized errors between model predicted knee abduction torque and experimentally obtained torque for toeout gait with 0.08 % body weight times height (BW*H) and 0.18 %BW*H errors for 1st and 2nd peaks, respectively (RMS for entire cycle = 0.14 %BW*H) (Figure 5-1, Table 5-4). Changes for hip torques were matched well (RMS = 0.48 %BW*H) with the exception a minor deviation (2.82 %BW*H) in the hip flexion-extension torque at the beginning of the cycle. Knee flexion-extension torque changes were matched with an RMS difference of 0.22 %BW*H. Both ankle torques remained close to the initial normal gait values (RMS = 0.02 %BW*H) without matching the small changes for toeout gait (RMS = 0.48 %BW*H). Overall changes for hip joint angles were matched (RMS = 4.11°) with the exception of internal-external rotation angle (max = 9.54° at 7% of cycle). The knee flexion-extension angle remained more flexed than necessary (RMS = 2.69°, max = 3.88° at 16% of cycle). Both ankle joint angles generally matched the changes well (RMS = 3.58°), but deviations were seen near 60% of cycle with a maximum of 9.67°. Other tracked quantities demonstrated good agreement (Table 5-5). All kinematic and kinetic differences are summarized in Table 5-7.

Using the control parameters tuned with toeout gait for the model calibrated with phases one, two, and three, the optimization predicted knee abduction torque for wide stance with RMS of 0.23 %BW*H (0.03 %BW*H and 0.11 %BW*H errors for 1st and 2nd peaks, respectively) (Figure 5-2, Table 5-4). Changes for hip torques were matched well (RMS = 0.46 %BW*H) with the exception a minor deviations (1.54 %BW*H at 4%

of cycle and 3.27 %BW*H at 100% of cycle) in the hip flexion-extension torque. Knee flexion-extension torque changes were matched with an RMS difference of 0.39 %BW*H. Both ankle torques remained close to the initial normal gait values (RMS = 0.008 %BW*H) without matching the small changes for wide stance gait (RMS = 0.36 %BW*H). Overall changes for hip joint angles were matched (RMS = 3.13°) with the maximum difference (7.81 %BW*H) occurring at 86% of cycle for the hip flexion-extension angle. The knee flexion-extension angle remained more extended than necessary (RMS = 3.06°, max = 3.31° at 76% of cycle, or 2nd peak). Both ankle joint angles generally matched the changes satisfactorily (RMS = 5.18°), but deviations were demonstrated near the end of cycle for both talocrural (max = 11.51° at 90% of cycle) and subtalar angles (max = 11.42° at 100% of cycle). Other tracked quantities demonstrated good agreement (Table 5-6). All kinematic and kinetic differences are summarized in Table 5-8.

There were noticeable effects when using dynamic models created without phase one or phase two of the optimization procedure. The resulting control parameters from phase three varied widely (Table 5-3). The predicted knee abduction torque for toeout gait showed considerable differences using models without phase one included, while the model prediction including phases one and three was comparable to the model with phases one, two, and three (Figure 5-1, Table 5-4). For wide stance gait, the knee abduction torque was not predicted well when using models without phase one, but the prediction including phases one and three showed some improvement (Figure 5-2, Table 5-4). In all cases, tracked quantities demonstrated good agreement (Table 5-5, Table 5-6). Concerning the virtual HTO, the sensitivities to wedge angle showed the expected

incremental reductions in knee abduction torque for only those models including phases one and three or phases one, two, and three (Figure 5-3). The differences in dynamic models created from different portions of the multi-phase optimization approach led to variations in the computed knee abduction torques for experimental and simulated data (Figure 5-4, Figure 5-5).

Discussion

The main motivation for developing a patient-specific inverse dynamics optimization approach is to predict novel patient-specific gait motions (e.g., subtle gait changes and HTO post-surgery gait). Toeout gait was successfully used to tune patient-specific control parameters. Wide stance gait predictions match the experiment rather well. The response surface approach greatly increased the computation efficiency of determining the control parameters.

The current approach has several limitations. A pin joint knee model was chosen to represent the flexion-extension motion that dominates other knee motions during gait. A rigid foot model without ground contact model was selected to increase the computational speed and exploit the ability to prescribe a desired foot path for the inverse dynamics optimization. A few kinematic and kinetic quantities were not predicted as well as others. Selection of tracking term weights is subjective and was performed in a manner to constrain the foot paths alone and track the other quantities. The control parameters identified during phase 3 depend on the weights chosen for the tracking terms. Although referred to as control parameters (joint torque = control), the cost function weights do not have an obvious physical explanation tied to neural control strategies.

It cannot be claimed that predictions made with this multi-phase approach will reproduce the actual functional outcome for every patient and every data set. This is

clear from the calibration results for toeout gait and the evaluation results for wide stance gait, where the RMS errors in the knee abduction torque predictions were not zero. At the same time, the predicted curves matched the 1st and 2nd peaks well. Thus, it can only be claimed that the optimized model structure provides the best possible prediction given the imperfect movement data inputs.

For the model calibrated with phase one and two, the optimization predictions for virtual HTO surgeries showed sensitivities in agreement with previous clinical studies (Bryan *et al.*, 1997, Wada *et al.*, 1998) (Figure 5-3). For the 3° case, the knee abduction torque was reduced by 0.78 %BW*H and 0.71 %BW*H for the 1st and 2nd peaks, respectively. Bryan *et al.* (1997) showed an approximately 1.1 %BW*H (slightly higher than optimization prediction) decrease for 3° of change. For the 5° case, the knee abduction torque was reduced by 0.95 %BW*H and 1.26 %BW*H for the 1st and 2nd peaks, respectively. Bryan *et al.* (1997) showed an approximately 1.2 %BW*H (very similar to optimization prediction) decrease for 5° of change. For the 7° case, the knee abduction torque was reduced by 1.23 %BW*H and 1.74 %BW*H for the 1st and 2nd peaks, respectively. Bryan *et al.* (1997) showed an approximately 1.5 %BW*H (slightly lower than optimization prediction) decrease for 7° of change.

Cost function weights calibrated to a particular gait motion accurately predict several kinematic and kinetic quantities for a different gait motion. Further investigation is necessary to determine the efficacy of the predictions for HTO. It would be advantageous to create patient-specific models and predictions for a population of HTO patients pre-surgery and compare with post-surgery outcome. Examination of different gaits (e.g., normal and pathological) requires future study as well.

Table 5-1. Descriptions of cost function weights and phase 3 control parameters.

Weight	Description
w_1	Scale factor for tracking foot paths
w_2	Scale factor for tracking pelvis transverse plane translations
w_3	Scale factor for tracking trunk orientations
w_4	Scale factor for tracking center of pressure translations
w_5	Scale factor for tracking residual pelvis forces and torques
w_6	Control parameter for tracking hip flexion-extension torque
w_7	Control parameter for tracking hip adduction-abduction torque
w_8	Control parameter for tracking hip internal-external torque
w_9	Control parameter for tracking knee flexion-extension torque
w_{10}	Control parameter for tracking talocrural dorsiflexion-plantarflexion torque
w_{11}	Control parameter for tracking subtalar inversion-eversion torque

Table 5-2. Summary of fixed offsets added to normal gait for each prescribed foot path.

Offset	Side	Toeout Gait	Wide Stance Gait
Anterior Translation (mm)	Right	41.78	-5.26
	Left	21.23	-3.50
Lateral Translation (mm)	Right	-28.45	62.57
	Left	-34.86	42.18
Transverse Plane Rotation (°)	Right	-15.79	-0.75
	Left	13.12	-0.29

Table 5-3. Comparison of cost function weights and phase 3 control parameters.

Weight	Phase 3 only	Phases 1 and 3	Phases 2 and 3	Phases 1, 2, and 3
w_1	10.00	10.00	10.00	10.00
w_2	1.00	1.00	1.00	1.00
w_3	1.00	1.00	1.00	1.00
w_4	1.00	1.00	1.00	1.00
w_5	1.00	1.00	1.00	1.00
w_6	8.71	5.79e-01	8.13	5.17
w_7	8.67	2.23	6.84	3.57e-01
w_8	7.31e-08	9.29e-10	7.18e-01	1.08
w_9	9.14	1.62e-07	6.74	2.94e-01
w_{10}	2.61	8.18	6.87	5.55
w_{11}	4.24	9.63	9.18	9.17

Table 5-4. Summary of root-mean-square (RMS) errors for predicted left knee abduction torque quantities for toeout and wide stance gait.

Gait trial	RMS error (% BW*H)			
	Phase 3 only	Phases 1 and 3	Phases 2 and 3	Phases 1, 2, and 3
Toeout	0.66	0.13	0.69	0.14
Wide stance	0.68	0.37	0.68	0.21

Table 5-5 Summary of root-mean-square (RMS) errors for tracked quantities for toeout gait.

Quantity	Description	RMS error			
		Phase 3 only	**Phases 1 and 3**	**Phases 2 and 3**	**Phases 1, 2, and 3**
$(q_{foot})_{right}$	6 DOFs for right prescribed foot path	2.55 mm 1.58°	3.64 mm 2.03°	1.53 mm 0.96°	2.35 mm 1.56°
$(q_{foot})_{left}$	6 DOFs for left prescribed foot path	0.94 mm 1.27°	2.02 mm 1.38°	0.57 mm 0.86°	1.36 mm 0.97°
q_{pelvis}	2 transverse plane translations for pelvis	7.65 mm	5.14 mm	9.91 mm	6.61 mm
q_{trunk}	3 DOFs for trunk orientation	0.32°	0.36°	0.52°	0.38°
$(CoP_{foot})_{right}$	2 transverse plane translations for right center of pressure	9.68 mm	9.78 mm	5.68 mm	7.30 mm
$(CoP_{foot})_{left}$	2 transverse plane translations for left center of pressure	2.01 mm	4.17 mm	1.68 mm	2.73 mm
F_{pelvis}	3 residual pelvis forces	4.23 N	4.27 N	3.82 N	4.11 N
T_{pelvis}	3 residual pelvis torques	3.93 Nm	3.37 Nm	2.99 Nm	2.41 Nm

Table 5-6. Summary of root-mean-square (RMS) errors for tracked quantities for wide stance gait.

Quantity	Description	RMS error			
		Phase 3 only	**Phases 1 and 3**	**Phases 2 and 3**	**Phases 1, 2, and 3**
$(q_{foot})_{right}$	6 DOFs for right prescribed foot path	1.07 mm 0.99°	1.19 mm 1.36°	0.85 mm 1.09°	0.45 mm 0.37°
$(q_{foot})_{left}$	6 DOFs for left prescribed foot path	0.99 mm 1.04 °	2.07 mm 1.29°	0.60 mm 1.16°	0.32 mm 0.24°
q_{pelvis}	2 transverse plane translations for pelvis	6.47 mm	6.42 mm	6.22 mm	7.33 mm
q_{trunk}	3 DOFs for trunk orientation	0.78°	0.83°	0.84°	0.75°
$(CoP_{foot})_{right}$	2 transverse plane translations for right center of pressure	4.45 mm	5.73 mm	4.74 mm	4.40 mm
$(CoP_{foot})_{left}$	2 transverse plane translations for left center of pressure	1.80 mm	1.74 mm	3.33 mm	0.79 mm
F_{pelvis}	3 residual pelvis forces	3.56 N	3.85 N	3.65 N	3.77 N
T_{pelvis}	3 residual pelvis torques	3.17 Nm	2.73 Nm	3.50 Nm	2.48 Nm

Table 5-7. Summary of root-mean-square (RMS) differences between optimization results and original normal gait or final toeout gait kinematic and kinetic quantities.

Quanitity	RMS difference from optimization							
	Phase 3 only		Phases 1 and 3		Phases 2 and 3		Phases 1, 2, and 3	
	Original	Final	Original	Final	Original	Final	Original	Final
Hip flexion angle (°)	1.29	3.22	9.14e-01	3.72	2.09	2.79	1.08	3.46
Hip abduction angle (°)	1.73	2.55	2.20	2.27	2.37	2.39	2.63	2.32
Hip rotation angle (°)	10.96	5.39	10.94	5.71	11.03	5.35	11.27	5.76
Knee flexion angle (°)	1.61	2.68	1.03	2.76	1.62	2.52	8.93e-01	2.69
Ankle flexion angle (°)	1.85	3.21	2.05	2.85	1.53	2.85	1.78	2.58
Ankle inversion angle (°)	4.43	4.71	3.89	4.49	4.14	4.87	3.49	4.36
Anterior center of pressure (mm)	11.35	15.09	2.45	9.89	1.29	9.97	1.58	9.33
Lateral center of pressure (mm)	22.41	23.35	5.36	9.27	1.99	7.09	3.53	7.86
Hip flexion torque (% BW*H)	2.49e-02	1.55	4.05e-01	9.39e-01	2.15e-02	1.55	3.11e-02	7.01e-01
Hip abduction torque (% BW*H)	1.70e-02	7.46e-01	9.58e-02	3.43e-01	2.43e-02	7.50e-01	2.31e-01	4.21e-01
Hip rotation torque (% BW*H)	1.62e-01	1.76e-01	1.42e-01	1.99e-01	1.12e-01	1.80e-01	1.10e-01	1.83e-01
Knee flexion torque (% BW*H)	1.67e-02	2.98e-01	3.75e-01	2.92e-01	1.50e-02	2.92e-01	2.41e-01	2.21e-01
Ankle flexion torque (% BW*H)	5.09e-02	1.27	3.24e-02	5.49e-01	1.41e-02	1.29	1.60e-02	5.53e-01
Ankle inversion torque (% BW*H)	3.92e-02	2.32	7.07e-02	3.98e-01	1.79e-02	2.31	2.98e-02	3.86e-01
Anterior ground reaction force (% BW)	2.33e-01	1.26	2.65e-01	1.31	5.16e-01	1.32	2.51e-01	1.39
Superior ground reaction force (% BW)	1.73	3.49	1.29	3.60	1.52	3.95	7.07e-01	4.04
Lateral ground reaction force (% BW)	6.98e-01	3.65e-01	5.43e-01	2.78e-01	7.58e-01	3.42e-01	5.64e-01	3.28e-01

Table 5-8. Summary of root-mean-square (RMS) differences between optimization results and original normal gait or final wide stance gait kinematic and kinetic quantities.

Quanitity	RMS difference from optimization							
	Phase 3 only		Phases 1 and 3		Phases 2 and 3		Phases 1, 2, and 3	
	Original	Final	Original	Final	Original	Final	Original	Final
Hip flexion angle (°)	6.64e-01	4.39	5.50e-01	4.55	3.68e-01	4.29	1.66	4.17
Hip abduction angle (°)	3.07	1.73	3.59	1.69	3.21	1.73	3.21	1.98
Hip rotation angle (°)	2.43	2.62	1.74	2.82	1.91	2.58	2.49	3.18
Knee flexion angle (°)	6.75e-01	3.46	1.48	4.41	6.28e-01	3.48	1.12	2.79
Ankle flexion angle (°)	2.17	4.35	2.19	5.18	1.91	4.33	2.08	5.17
Ankle inversion angle (°)	6.82	6.43	4.06	4.07	5.87	5.53	5.00	4.72
Anterior center of pressure (mm)	1.44	27.40	1.49	26.01	4.45	27.52	1.05	26.31
Lateral center of pressure (mm)	2.10	11.22	1.95	9.13	1.54	11.22	3.68e-01	8.18
Hip flexion torque (% BW*H)	2.33e-02	5.04e-01	1.71e-01	5.95e-01	2.43e-02	5.25e-01	1.58e-02	6.26e-01
Hip abduction torque (% BW*H)	3.82e-02	5.25e-01	1.29e-01	3.39e-01	6.54e-02	5.21e-01	2.53e-01	3.23e-01
Hip rotation torque (% BW*H)	1.93e-01	2.44e-01	2.10e-01	2.87e-01	2.00e-01	2.49e-01	9.11e-02	2.48e-01
Knee flexion torque (% BW*H)	1.28e-02	4.27e-01	2.49e-01	6.24e-01	1.46e-02	4.37e-01	2.79e-01	3.90e-01
Ankle flexion torque (% BW*H)	1.85e-02	3.74e-01	1.15e-02	3.91e-01	1.01e-02	3.71e-01	1.07e-02	3.93e-01
Ankle inversion torque (% BW*H)	3.16e-02	4.23e-01	2.53e-02	3.45e-01	1.62e-02	4.23e-01	2.39e-02	3.63e-01
Anterior ground reaction force (% BW)	2.76e-01	1.13	3.94e-01	1.20	2.81e-01	1.17	6.76e-01	1.04
Superior ground reaction force (% BW)	1.03	4.15	8.09e-01	3.98	1.23	4.30	2.13	3.93
Lateral ground reaction force (% BW)	2.66	8.75e-01	2.35	1.14	2.56	8.72e-01	1.75	1.79

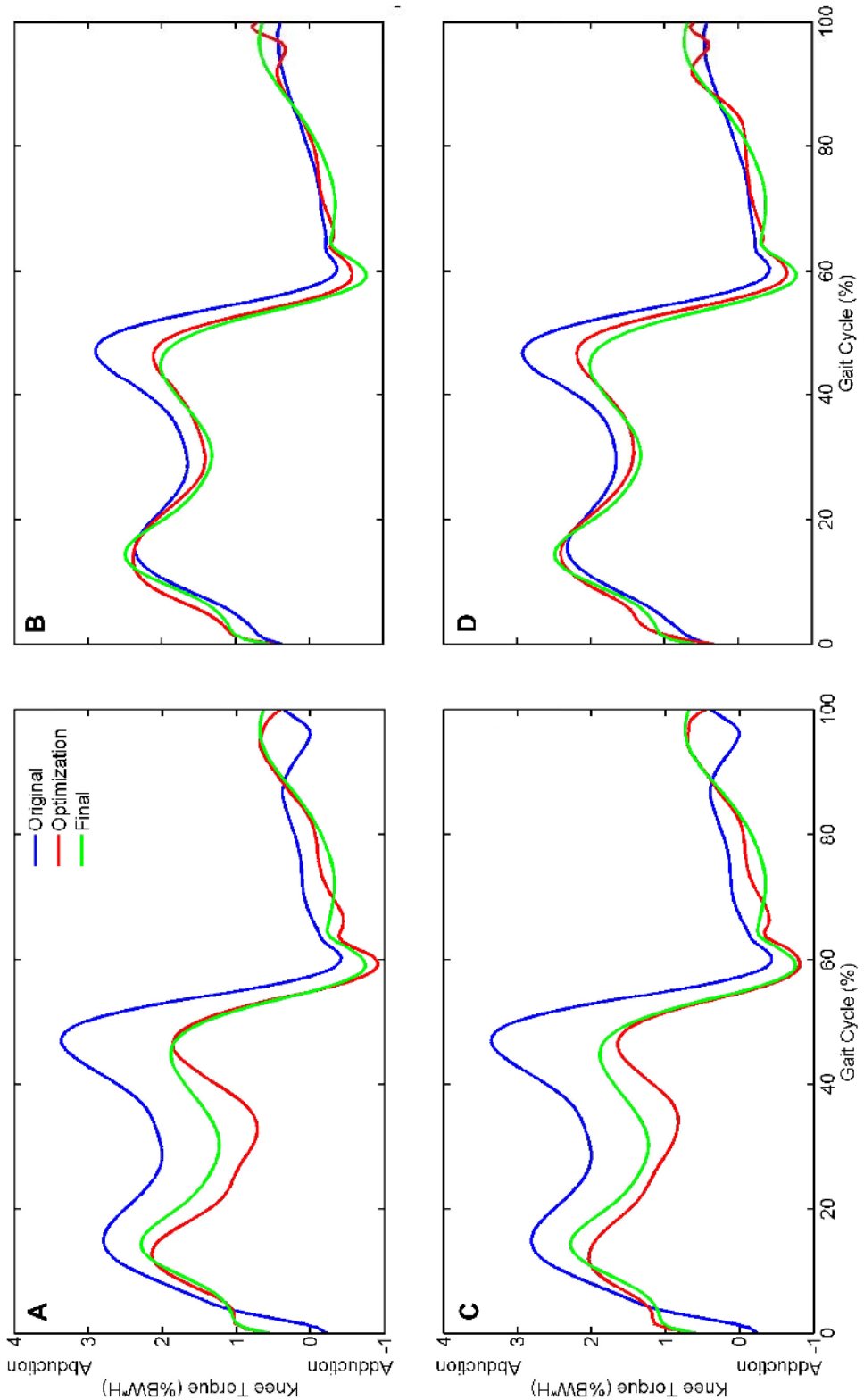

Figure 5-1. Comparison of left knee abduction torques for toeout gait. Original (blue) is experimental normal gait, simulation (red) is predicted toeout gait, and final (green) is experimental toeout gait. Plot A) contains curves for model using phase 3 only. Plot B) contains curves for model using phases 1 and 3. Plot C) contains curves for model using phases 2 and 3. Plot D) contains curves for model using phases 1, 2, and 3.

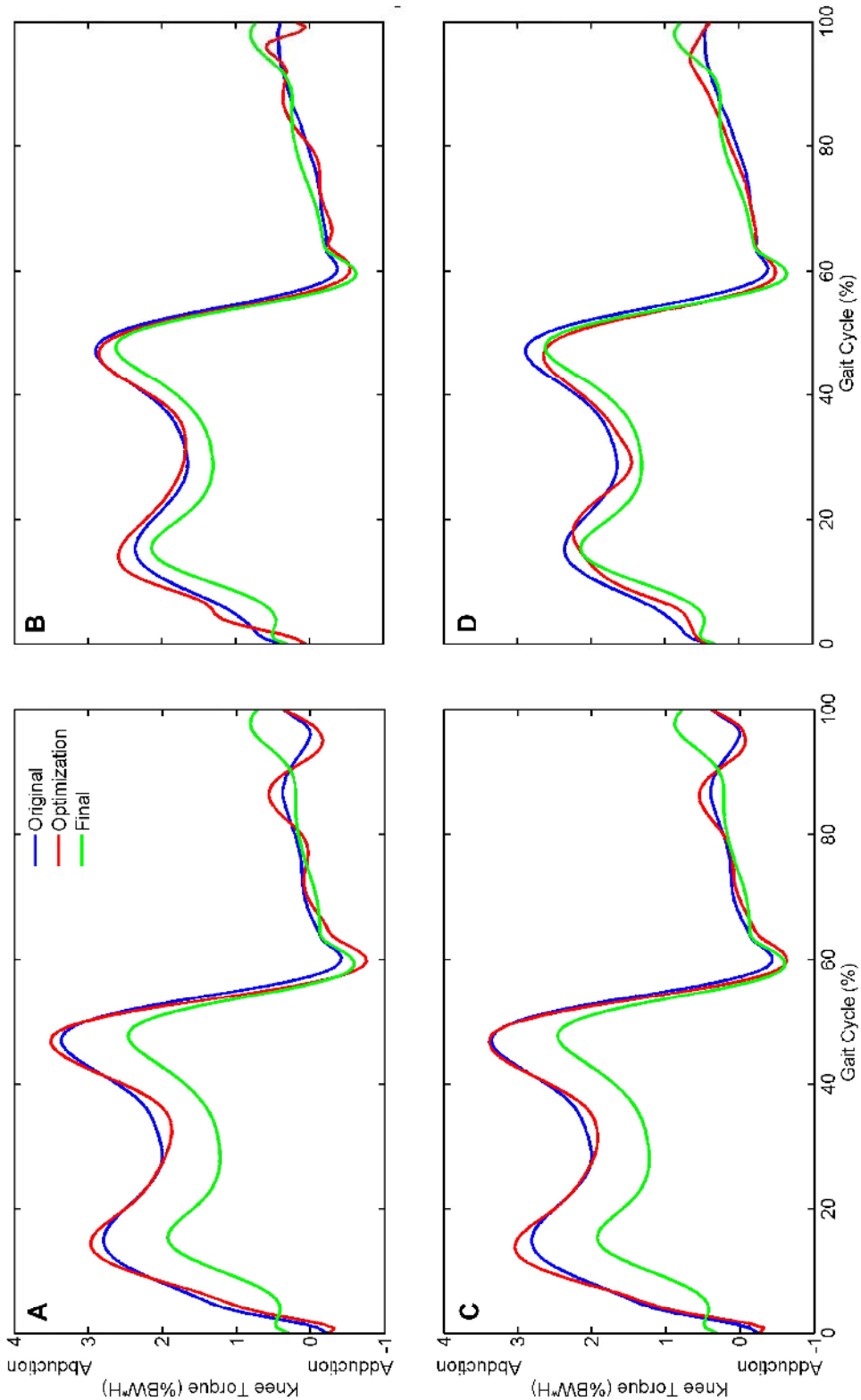

Figure 5-2. Comparison of left knee abduction torques for wide stance gait, where original (blue) is experimental normal gait, simulation (red) is predicted toeout gait, and final (green) is experimental toeout gait. Plot A) contains curves for model using phase 3 only. Plot B) contains curves for model using phases 1 and 3. Plot C) contains curves for model using phases 2 and 3. Plot D) contains curves for model using phases 1, 2, and 3.

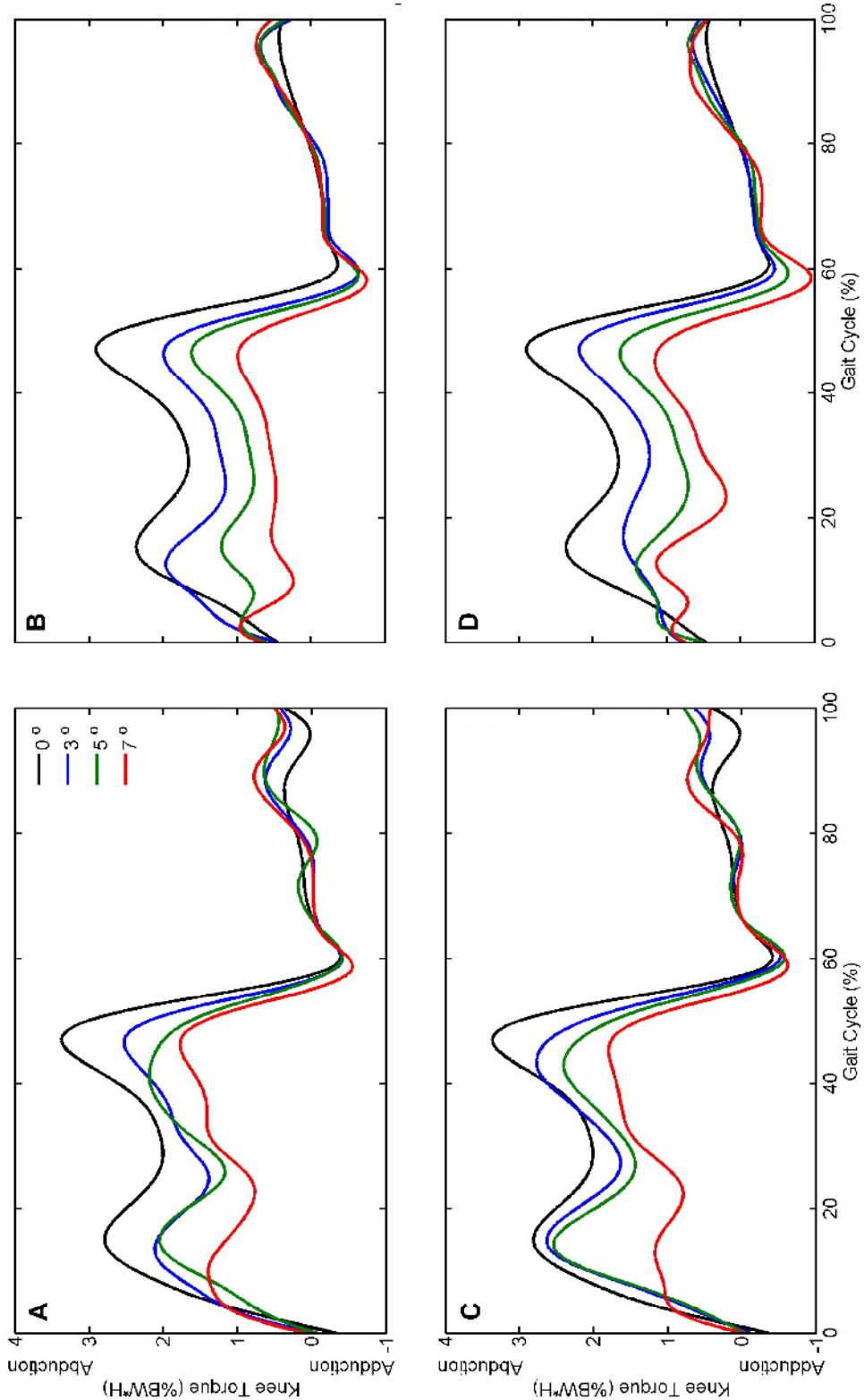

Figure 5-3. Comparison of left knee abduction torques for simulated high tibial osteotomy (HTO) post-surgery gait. Plot A) contains curves for model using phase 3 only. Plot B) contains curves for model using phases 1 and 3. Plot C) contains curves for model using phases 2 and 3. Plot D) contains curves for model using phases 1, 2, and 3.

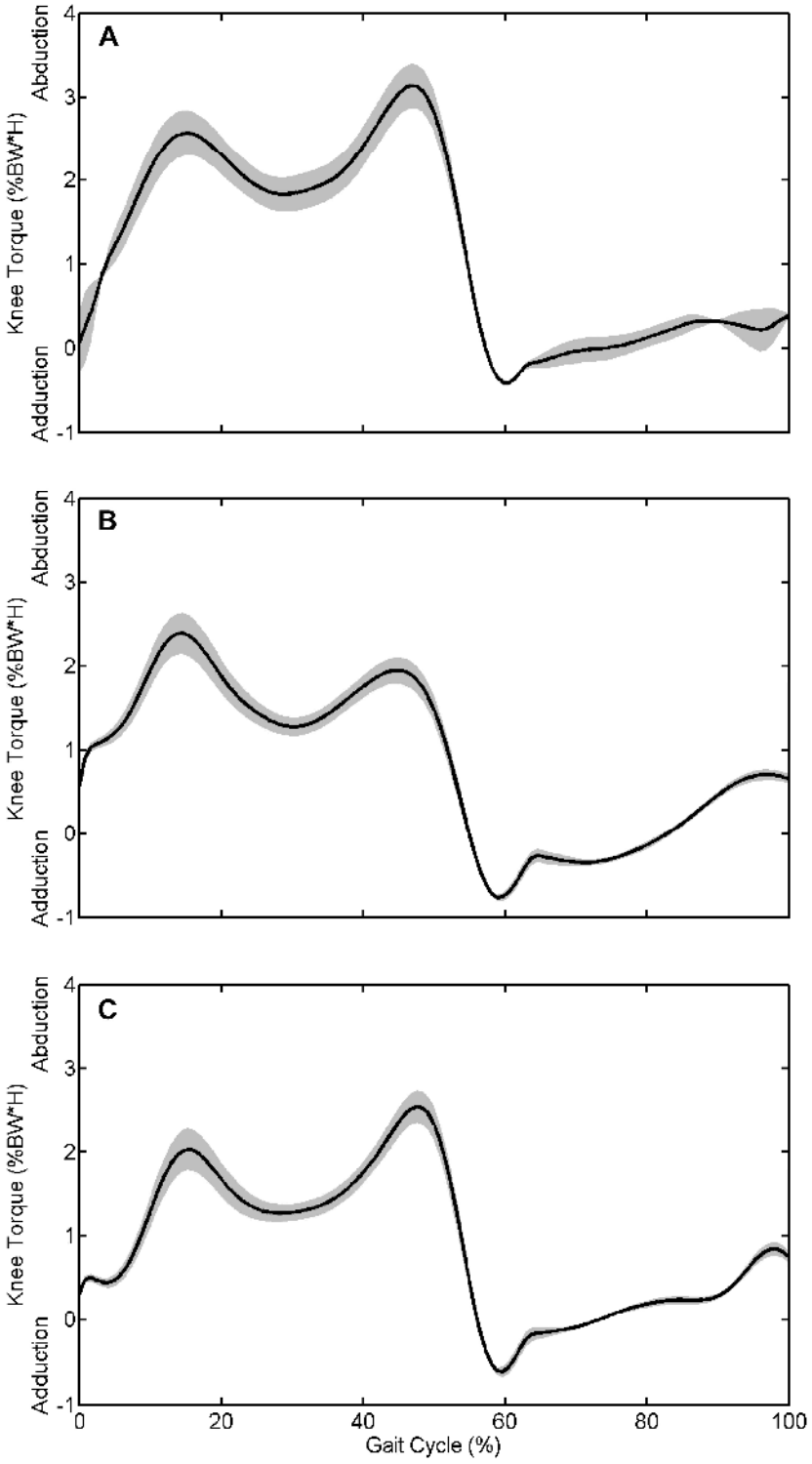

Figure 5-4. Comparison of mean (solid black line) plus or minus one standard deviation (gray shaded area) for experimental left knee abduction torques. Plot A) contains distribution for normal gait. Plot B) contains distribution for toeout gait. Plot C) contains distribution for wide stance gait.

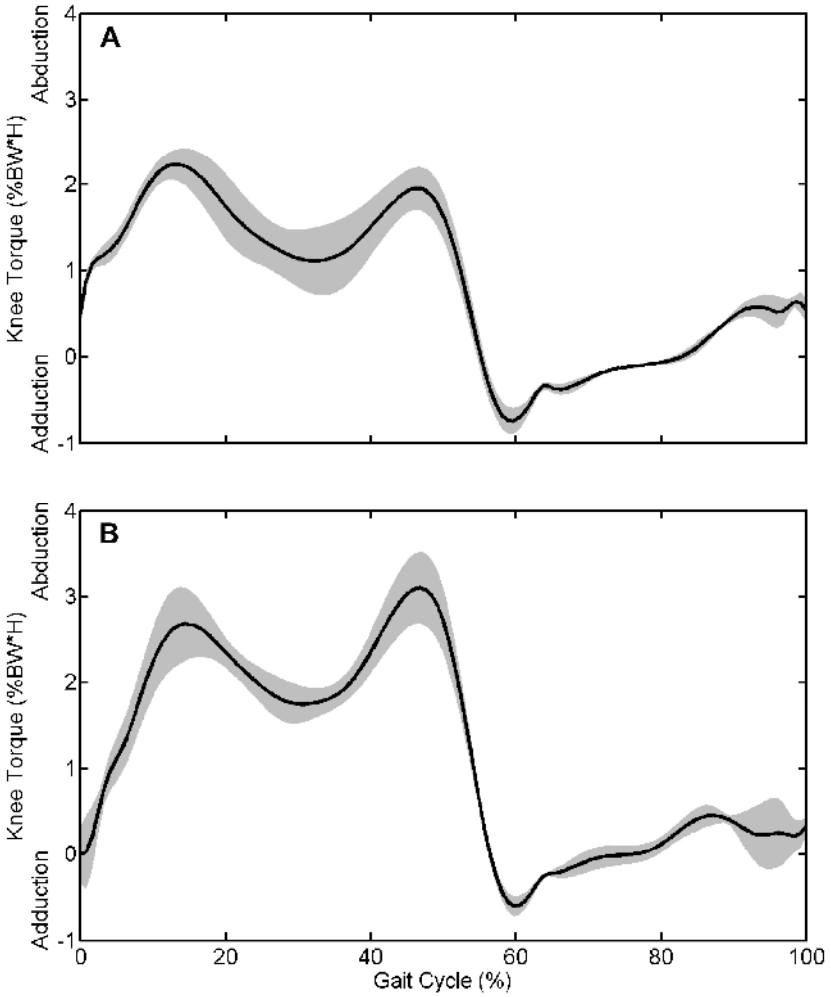

Figure 5-5. Comparison of mean (solid black line) plus or minus one standard deviation (gray shaded area) for simulated left knee abduction torques. Plot A) contains distribution for toeout gait. Plot B) contains distribution for wide stance gait.

CHAPTER 6
CONCLUSION

Rationale for New Approach

The main motivation for developing a 27 DOF patient-specific inverse dynamic model and the associated optimization approach is to predict the post-surgery peak external knee adduction moment in HTO patients, which has been identified as an indicator of clinical outcome (Andriacchi, 1994; Bryan *et al.*, 1997; Hurwitz *et al.*, 1998; Prodromos *et al.*, 1985; Wang *et al.*, 1990). The accuracy of prospective dynamic analyses made for a unique patient is determined in part by the fitness of the underlying kinematic and kinetic model (Andriacchi and Strickland, 1985; Challis and Kerwin, 1996; Cappozzo and Pedotti, 1975; Davis, 1992; Holden and Stanhope, 1998; Holden and Stanhope, 2000; Stagni *et al.*, 2000). Development of an accurate model tailored to a specific patient forms the foundation for creating a predictive patient-specific dynamic simulation.

Synthesis of Current Work and Literature

The multi-phase optimization method satisfactorily determines patient-specific model parameters defining a 3D model that is well suited to a particular patient. Two conclusions may be drawn from comparing and contrasting the optimization results to previous values found in the literature. The similarities between numbers suggest the results are reasonable and show the extent of agreement with past studies. The differences between values indicate the optimization is necessary and demonstrate the degree of inaccuracy inherent when the new approach is not implemented. Through the

enhancement of model parameter values found in the literature, the multi-phase optimization approach successfully reduces the fitness errors between the patient-specific model and the experimental motion data.

The precision of dynamic analyses made for a particular patient depends on the accuracy of the patient-specific kinematic and kinetic parameters chosen for the dynamic model. Without expensive medical images, model parameters are only estimated from external landmarks that have been identified in previous studies. The estimated (or nominal) values may be improved by formulating an optimization problem using motion-capture data. By using a multi-phase optimization technique, researchers may build more accurate biomechanical models of the individual human structure. As a result, the optimal models will provide reliable foundations for dynamic analyses and optimizations.

Simulations based on inverse dynamics optimization subject to reality constraints predict physics-based motion. The results accurately represent a specific patient within the bounds of the chosen dynamic model, experimental task, and data quality. Given the agreement of the current results with previous studies, there is significant benefit in the construction and optimization a patient-specific functional dynamic model to assist in the planning and outcome prediction of surgical procedures. This work comprises a unique computational framework to create and apply objective patient-specific models (different from current intuitive models based on clinical experience or regression models based on population studies) to predict clinically significant outcomes.

GLOSSARY

Abduction	Movement away from the midline of the body in the coronal plane.
Acceleration	The time rate of change of velocity.
Active markers	Joint and segment markers used during motion capture that emit a signal.
Adduction	Movement towards the midline of the body in the coronal plane.
Ankle inversion-eversion	Motion of the long axis of the foot within the coronal plane as seen by an observer positioned along the anterior-posterior axis of the shank.
Ankle motion	The ankle angles reflect the motion of the foot segment relative to the shank segment.
Ankle plantarflexion-dorsiflexion	Motion of the plantar aspect of the foot within the sagittal plane as seen by an observer positioned along the medial-lateral axis of the shank.
Anterior	The front or before, also referred to as ventral.
Coccyx	The tailbone located at the distal end of the sacrum.
Constraint functions	Specific limits that must be satisfied by the optimal design.
Coronal plane	The plane that divides the body or body segment into anterior and posterior parts.
Degree of freedom (DOF)	A single coordinate of relative motion between two bodies. Such a coordinate responds without constraint or imposed motion to externally applied forces or torques. For translational motion, a DOF is a linear coordinate along a single direction. For rotational motion, a DOF is an angular coordinate about a single, fixed axis.

Design variables	Variables that change to optimize the design.
Distal	Away from the point of attachment or origin.
Dorsiflexion	Movement of the foot towards the anterior part of the tibia in the sagittal plane.
Epicondyle	Process that develops proximal to an articulation and provides additional surface area for muscle attachment.
Eversion	A turning outward.
Extension	Movement that rotates the bones comprising a joint away from each other in the sagittal plane.
External (lateral) rotation	Movement that rotates the distal segment laterally in relation to the proximal segment in the transverse plane, or places the anterior surface of a segment away from the longitudinal axis of the body.
External moment	The load applied to the human body due to the ground reaction forces, gravity and external forces.
Femur	The longest and heaviest bone in the body. It is located between the hip joint and the knee joint.
Flexion	Movement that rotates the bones comprising a joint towards each other in the sagittal plane.
Force	A push or a pull and is produced when one object acts on another.
Force plate	A transducer that is set in the floor to measure about some specified point, the force and torque applied by the foot to the ground. These devices provide measures of the three components of the resultant ground reaction force vector and the three components of the resultant torque vector.
Forward dynamics	Analysis to determine the motion of a mechanical system, given the topology of how bodies are connected, the applied forces and torques, the mass properties, and the initial condition of all degrees of freedom.

Gait	A manner of walking or moving on foot.
Generalized coordinates	A set of coordinates (or parameters) that uniquely describes the geometric position and orientation of a body or system of bodies. Any set of coordinates that are used to describe the motion of a physical system.
High tibial osteotomy (HTO)	Surgical procedure that involves adding or removing a wedge of bone to or from the tibia and changing the frontal plane limb alignment. The realignment shifts the weight-bearing axis from the diseased medial compartment to the healthy lateral compartment of the knee.
Hip abduction-adduction	Motion of a long axis of the thigh within the coronal plane as seen by an observer positioned along the anterior-posterior axis of the pelvis.
Hip flexion-extension	Motion of the long axis of the thigh within the sagittal plane as seen by an observer positioned along the medial-lateral axis of the pelvis.
Hip internal-external rotation	Motion of the medial-lateral axis of the thigh with respect to the medial-lateral axis of the pelvis within the transverse plane as seen by an observer positioned along the longitudinal axis of the thigh.
Hip motion	The hip angles reflect the motion of the thigh segment relative to the pelvis.
Inferior	Below or at a lower level (towards the feet).
Inter-ASIS distance	The length of measure between the left anterior superior iliac spine (ASIS) and the right ASIS.
Internal (medial) rotation	Movement that rotates the distal segment medially in relation to the proximal segment in the transverse plane, or places the anterior surface of a segment towards the longitudinal axis of the body.
Internal joint moments	The net result of all the internal forces acting about the joint which include moments due to muscles, ligaments, joint friction and structural constraints.

	The joint moment is usually calculated around a joint center.
Inverse dynamics	Analysis to determine the forces and torques necessary to produce the motion of a mechanical system, given the topology of how bodies are connected, the kinematics, the mass properties, and the initial condition of all degrees of freedom.
Inversion	A turning inward.
Kinematics	Those parameters that are used in the description of movement without consideration for the cause of movement abnormalities. These typically include parameters such as linear and angular displacements, velocities and accelerations.
Kinetics	General term given to the forces that cause movement. Both internal (muscle activity, ligaments or friction in muscles and joints) and external (ground or external loads) forces are included. The moment of force produced by muscles crossing a joint, the mechanical power flowing to and from those same muscles, and the energy changes of the body that result from this power flow are the most common kinetic parameters used.
Knee abduction-adduction	Motion of the long axis of the shank within the coronal plane as seen by an observer positioned along the anterior-posterior axis of the thigh.
Knee flexion-extension	Motion of the long axis of the shank within the sagittal plane as seen by an observer positioned along the medial-lateral axis of the thigh.
Knee internal-external rotation	Motion of the medial-lateral axis of the shank with respect to the medial-lateral axis of the thigh within the transverse plane as viewed by an observer positioned along the longitudinal axis of the shank.
Knee motion	The knee angles reflect the motion of the shank segment relative to the thigh segment.
Lateral	Away from the body's longitudinal axis, or away from the midsagittal plane.

Malleolus	Broadened distal portion of the tibia and fibula providing lateral stability to the ankle.
Markers	Active or passive objects (balls, hemispheres or disks) aligned with respect to specific bony landmarks used to help determine segment and joint position in motion capture.
Medial	Toward the body's longitudinal axis, or toward the midsagittal plane.
Midsagittal plane	The plane that passes through the midline and divides the body or body segment into the right and left halves.
Model parameters	A set of coordinates that uniquely describes the model segments lengths, joint locations, and joint orientations, also referred to as joint parameters. Any set of coordinates that are used to describe the geometry of a model system.
Moment of force	The moment of force is calculated about a point and is the cross product of a position vector from the point to the line of action for the force and the force. In two-dimensions, the moment of force about a point is the product of a force and the perpendicular distance from the line of action of the force to the point. Typically, moments of force are calculated about the center of rotation of a joint.
Motion capture	Interpretation of computerized data that documents an individual's motion.
Objective functions	Figures of merit to be minimized or maximized.
Parametric	Of or relating to or in terms of parameters, or factors that define a system.
Passive markers	Joint and segment markers used during motion capture that reflect visible or infrared light.
Pelvis	Consists of the two hip bones, the sacrum, and the coccyx. It is located between the proximal spine and the hip joints.

Pelvis anterior-posterior tilt	Motion of the long axis of the pelvis within the sagittal plane as seen by an observer positioned along the medial-lateral axis of the laboratory.
Pelvis elevation-depression	Motion of the medial-lateral axis of the pelvis within the coronal plane as seen by an observer positioned along the anterior-posterior axis of the laboratory.
Pelvis internal-external rotation	Motion of the medial-lateral or anterior-posterior axis of the pelvis within the transverse plane as seen by an observer positioned along the longitudinal axis of the laboratory.
Pelvis motion	The position of the pelvis as defined by a marker set (for example, plane formed by the markers on the right and left anterior superior iliac spine (ASIS) and a marker between the 5^{th} lumbar vertebrae and the sacrum) relative to a laboratory coordinate system.
Plantarflexion	Movement of the foot away from the anterior part of the tibia in the sagittal plane.
Posterior	The back or behind, also referred to as dorsal.
Proximal	Toward the point of attachment or origin.
Range of motion	Indicates joint motion excursion from the maximum angle to the minimum angle.
Sacrum	Consists of the fused components of five sacral vertebrae located between the 5^{th} lumbar vertebra and the coccyx. It attaches the axial skeleton to the pelvic girdle of the appendicular skeleton via paired articulations.
Sagittal plane	The plane that divides the body or body segment into the right and left parts.
Skin movement artifacts	The relative movement between skin and underlying bone.
Stance phase	The period of time when the foot is in contact with the ground.

Subtalar joint	Located between the distal talus and proximal calcaneous, also known as the talocalcaneal joint.
Superior	Above or at a higher level (towards the head).
Synthetic markers	Computational representations of passive markers located on the kinematic model.
Swing phase	The period of time when the foot is not in contact with the ground.
Talocrural joint	Located between the distal tibia and proximal talus, also known as the tibial-talar joint.
Talus	The largest bone of the ankle transmitting weight from the tibia to the rest of the foot.
Tibia	The large medial bone of the lower leg, also known as the shinbone. It is located between the knee joint and the talocrural joint.
Transepicondylar	The line between the medial and lateral epicondyles.
Transverse plane	The plane at right angles to the coronal and sagittal planes that divides the body into superior and inferior parts.
Velocity	The time rate of change of displacement.

LIST OF REFERENCES

Andrews, J.G., and Mish, S.P., 1996. "Methods for Investigating the Sensitivity of Joint Resultants to Body Segment Parameter Variations." *Journal of Biomechanics*, Volume 29, Number 5, Pages 651-654.

Andriacchi, T.P., 1994. "Dynamics of Knee Malalignment." *Orthopedic Clinics of North America*, Volume 25, Number 3, Pages 395-403.

Andriacchi, T.P., and Strickland, A.B., 1985. "Gait Analysis as a Tool to Assess Joint Kinetics." In: Berme, N., Engin, A.E., Correia da Silva, K.M. (Editors), *Biomechanics of Normal and Pathological Human Articulating Joints*. Martinus Nijhoff Publishers, Dordrecht, The Netherlands, Pages 83-102.

Arnold, A.S, Asakawa, D.J, and Delp, S.L., 2000. "Do the Hamstrings and Adductors Contribute to Excessive Internal Rotation of the Hip in Persons with Cerebral Palsy?" *Gait & Posture*, Volume 11, Number 3, Pages 181-190.

Arnold, A.S., and Delp, S.L., 2001. "Rotational Moment Arms of the Hamstrings and Adductors Vary with Femoral Geometry and Limb Position: Implications for the Treatment of Internally-Rotated Gait." *Journal of Biomechanics*, Volume 34, Number 4, Pages 437-447.

Bell, A.L., Pedersen, D.R., and Brand, R.A., 1990. "A Comparison of the Accuracy of Several Hip Center Location Prediction Methods." *Journal of Biomechanics*, Volume 23, Number 6, Pages 617-621.

Bogert, A.J. van den, Smith, G.D., and Nigg, B.M., 1994. "In Vivo Determination of the Anatomical Axes of the Ankle Joint Complex: An Optimization Approach." *Journal of Biomechanics*, Volume 27, Number 12, Pages 1477-1488.

Bryan, J.M., Hurwitz, D.E., Bach, B.R., Bittar, T., and Andriacchi, T.P., 1997. "A Predictive Model of Outcome in High Tibial Osteotomy." In *Proceedings of the 43rd Annual Meeting of the Orthopaedic Research Society*, San Francisco, California, February 9-13, Volume 22, Paper 718.

Cappozzo, A., Catani, F., and Leardini, A., 1993. "Skin Movement Artifacts in Human Movement Photogrammetry." In *Proceedings of the XIVth Congress of the International Society of Biomechanics*, Paris, France, July 4-8, Pages 238-239.

Cappozzo, A., Leo, T., and Pedotti, A., 1975. "A General Computing Method for the Analysis of Human Locomotion." *Journal of Biomechanics*, Volume 8, Number 5, Pages 307-320.

Center for Disease Control (CDC), 2003. *Targeting Arthritis: The Nation's Leading Cause of Disability*. Centers for Disease Control and Prevention, National Center for Chronic Disease Prevention and Health Promotion, Atlanta, Georgia. Accessed: http://www.cdc.gov/nccdphp/aag/pdf/aag_arthritis2003.pdf, February, 2003.

Challis, J.H., and Kerwin, D.G., 1996. "Quantification of the Uncertainties in Resultant Joint Moments Computed in a Dynamic Activity." *Journal of Sports Sciences*, Volume 14, Number 3, Pages 219-231.

Chang, P.B., Williams, B.J., Santer, T.J., Notz, W.I., and Bartel, D.L., 1999. "Robust Optimization of Total Joint Replacements Incorporating Environmental Variables." *Journal of Biomechanical Engineering*, Volume 121, Number 3, Pages 304-310.

Chao, E.Y., and Sim, F.H., 1995. "Computer-Aided Pre-Operative Planning in Knee Osteotomy." *Iowa Orthopedic Journal*, Volume 15, Pages 4-18.

Chao, E.Y.S., Lynch, J.D., and Vanderploeg, M.J., 1993. "Simulation and Animation of Musculoskeletal Joint System. *Journal of Biomechanical Engineering*, Volume 115, Number 4, Pages 562-568.

Chéze, L., Fregly, B.J., and Dimnet, J., 1995. "A Solidification Procedure to Facilitate Kinematic Analyses Based on Video System Data." *Journal of Biomechanics*, Volume 28, Number 7, Pages 879-884.

Chéze, L., Fregly, B.J., and Dimnet, J., 1998. "Determination of Joint Functional Axes from Noisy Marker Data Using the Finite Helical Axis." *Human Movement Science*, Volume 17, Number 1, Pages 1-15.

Churchill, D.L., Incavo, S.J., Johnson, C.C., and Beymnon, B.D., 1998. "The Transepicondylar Axis Approximates the Optimal Flexion Axis of the Knee." *Clinical Orthopaedics and Related Research*, Volume 356, Number 1, Pages 111-118.

Croce, U.D., Leardini, A., Lorenzo, C., Cappozzo, A., 2005. "Human Movement Analysis Using Stereophotogrammetry Part 4: Assessment of Anatomical Landmark Misplacement and Its Effects on Joint Kinematics." *Gait and Posture*, Volume 21, Number 2, Pages 226-237.

Davis, B.L., 1992. "Uncertainty in Calculating Joint Moments During Gait." In *Proceedings of the 8th Meeting of European Society of Biomechanics*, Rome, Italy, June 21-24, Page 276.

de Leva, P., 1996. "Adjustments to Zatsiorsky-Seluyanov's Segment Inertia Parameters." *Journal of Biomechanics*, Volume 29, Number 9, Pages 1223-1230.

Delp, S.L., Arnold, A.S., and Piazza, S.J., 1998. "Graphics-Based Modeling and Analysis of Gait Abnormalities." *Bio-Medical Materials and Engineering*, Volume 8, Number 3/4, Pages 227-240.

Delp, S.L., Arnold, A.S., Speers, R.A., and Moore, C.A., 1996. "Hamstrings and Psoas Lengths During Normal and Crouch Gait: Implications for Muscle-Tendon Surgery." *Journal of Orthopaedic Research*, Volume 14, Number 1, Pages 144-151.

Delp, S.L., Loan, J.P., Hoy, M.G., Zajac, F.E., Topp E.L., and Rosen, J.M., 1990. "An Interactive Graphics-Based Model of the Lower Extremity to Study Orthopaedic Surgical Procedures." *IEEE Transactions on Biomedical Engineering*, Volume 37, Number 8, Pages 757-767.

Fantozzi, S., Stagni, R., Cappello, A., and Leardini, A., 2005. "Effect of Different Inertial Parameter Sets on Joint Moment Calculation During Stair Ascending and Descending." *Medical Engineering & Physics*, Volume 27, Pages 537-541

Fishman, G.S., 1996. *Monte Carlo: Concepts, Algorithms, and Applications*. Springer-Verlag New York, Inc., New York, NY.

Fregly, B.J., Rooney, K.L., and Reinbolt, J. A., 2005. "Predicted Gait Modifications to Reduce the Peak Knee Adduction Torque." In *Proceedings of the XXth Congress of the International Society of Biomechanics and 29th Annual Meeting of the American Society of Biomechanics*, Cleveland, Ohio, July 31-August 5, Page 283.

Griewank, A., 2000. "Evaluating Derivatives: Principles and Techniques of Algorithmic Differentiation." Society for Industrial and Applied Mathematics, Philadelphia, PA.

Griewank, A., Juedes, D., and Utke, J., 1996. "ADOL-C: a Package for the Automatic Differentiation of Algorithms Written in C/C++." *Association for Computing Machinery Transactions on Mathematical Software*, Volume 22, Number 2, Pages 131-167.

Heck, D.A., Melfi, C.A., Mamlin, L.A., Katz, B.P., Arthur, D.S., Dittus, R.S., and Freund, D.A., 1998. "Revision Rates Following Knee Replacement in the United States." *Medical Care*, Volume 36, Number 5, Pages 661-689.

Holden, J.P., and Stanhope, S.J., 1998. "The Effect of Variation in Knee Center Location Estimates on Net Knee Joint Moments." *Gait & Posture*, Volume 7, Number 1, Pages 1-6.

Holden, J.P., and Stanhope, S.J., 2000. "The Effect of Uncertainty in Hip Center Location Estimates on Hip Joint Moments During Walking at Different Speeds." *Gait & Posture*, Volume 11, Number 2, Pages 120-121.

Hong, J.H., Mun, M.S., and Song, S.H., 2001. "An Optimum Design Methodology Development Using a Statistical Technique for Vehicle Occupant Safety." In *Proceedings of the Institution of Mechanical Engineers, Part D: Journal of Automobile Engineering*, Volume 215, Number 7, Pages 795-801.

Hurwitz, D.E., Sumner, D.R., Andriacchi, T.P., and Sugar, D.A., 1998. "Dynamic Knee Loads During Gait Predict Proximal Tibial Bone Distribution." *Journal of Biomechanics*, Volume 31, Number 5, Pages 423-430.

Inman, V.T., 1976. *The Joints of the Ankle*. Williams and Wilkins Company, Baltimore, Maryland.

Lane, G.J., Hozack, W.J., Shah, S., Rothman, R.H., Booth, R.E. Jr., Eng, K., Smith, P., 1997. "Simultaneous Bilateral Versus Unilateral Total Knee Arthroplasty. Outcomes Analysis." *Clinical Orthopaedics and Related Research*, Volume 345, Number 1, Pages 106-112.

Leardini, A., Cappozzo, A., Catani, F., Toksvig-Larsen, S., Petitto, A., Sforza, V., Cassanelli, G., and Giannini, S., 1999. "Validation of a Functional Method for the Estimation of Hip Joint Centre Location." *Journal of Biomechanics*, Volume 32, Number 1, Pages 99-103.

Lu, T.-W., and O'Connor, J.J., 1999. "Bone Position Estimation from Skin Marker Coordinates Using Global Optimisation with Joint Constraints." *Journal of Biomechanics*, Volume 32, Number 2, Pages 129-134.

Manal, K., and Guo, M., 2005. "Foot Progression Angle and the Knee Adduction Moment in Individuals with Medial Knee Osteoarthritis." In *Proceedings of the XXth Congress of the International Society of Biomechanics and 29th Annual Meeting of the American Society of Biomechanics*, Cleveland, Ohio, July 31-August 5, Page 899.

Pandy, M.G., 2001. "Computer Modeling and Simulation of Human Movement." *Annual Reviews in Biomedical Engineering*, Volume 3, Number 1, Pages 245-273.

Pearsall D.J., and Costigan P.A., 1999. "The Effect of Segment Parameter Error on Gait Analysis Results." *Gait and Posture*, Volume 9, Number 3, Pages 173-183.

Prodromos, C.C., Andriacchi, T.P., and Galante, J.O., 1985. "A Relationship Between Gait and Clinical Changes Following High Tibial Osteotomy." *Journal of Bone Joint Surgery (American)*, Volume 67, Number 8, Pages 1188-1194.

Reinbolt, J.A., and Fregly, B.J., 2005. "Creation of Patient-Specific Dynamic Models from Three-Dimensional Movement Data Using Optimization." In *Proceedings of the 10th International Symposium on Computer Simulation in Biomechanics*, Cleveland, OH, July 28-30.

Reinbolt, J.A., Schutte, J.F., Fregly, B.J., Haftka, R.T., George, A.D., and Mitchell, K.H., 2005. "Determination of Patient-Specific Multi-Joint Kinematic Models Through Two-Level Optimization." *Journal of Biomechanics*, Volume 38, Number 3, Pages 621-626.

Sommer III, H.J., and Miller, N.R., 1980. "A Technique for Kinematic Modeling of Anatomical Joints." *Journal of Biomechanical Engineering*, Volume 102, Number 4, Pages 311-317.

Stagni, R., Leardini, A., Benedetti, M.G., Cappozzo, A., and Cappello, A., 2000. "Effects of Hip Joint Centre Mislocation on Gait Analysis Results." *Journal of Biomechanics*, Volume 33, Number 11, Pages 1479-1487.

Tetsworth, K., and Paley, D., 1994. "Accuracy of Correction of Complex Lower-Extremity Deformities by the Ilizarov Method." *Clinical Orthopaedics and Related Research*, Volume 301, Number 1, Pages 102-110.

Valero-Cuevas, F.J., Johanson, M.E., and Towles, J.D., 2003. "Towards a Realistic Biomechanical Model of the Thumb: the Choice of Kinematic Description May Be More Critical Than the Solution Method or the Variability/Uncertainty of Musculoskeletal Parameters." *Jouirnal of Biomechanics*, Volume 36, Number 7, Pages 1019-1030.

Vaughan, C.L., Andrews, J.G., and Hay, J.G., 1982. "Selection of Body Segment Parameters by Optimization Methods." *Journal of Biomechanical Engineering*, Volume 104, Number 1, Pages 38-44.

Wada, M., Imura, S., Nagatani, K., Baba, H., Shimada, S., and Sasaki, S., 1998. "Relationship Between Gait and Clinical Results After High Tibial Osteotomy." *Clinical Orthopaedics and Related Research*, Volume 354, Number 1, Pages 180-188.

Wang, J.-W., Kuo, K.N., Andriacchi, T.P., and Galante, J.O., 1990. "The Influence of Walking Mechanics and Time on the Results of Proximal Tibial Osteotomy." *Journal of Bone and Joint Surgery* (American), Volume 72, Number 6, Pages 905-913.

Winter, D.A., 1980. "Overall Principle of Lower Limb Support During Stance Phase of Gait." *Journal of Biomechanics*, Volume 13, Number 11, Pages 923-927.

BIOGRAPHICAL SKETCH

Jeffrey A. Reinbolt was born on May 6, 1974, in Bradenton, Florida. His parents are Charles and Joan Reinbolt. He has an older brother, Douglas, and an older sister, Melissa. In 1992, Jeff graduated salutatorian from Southeast High School, Bradenton, Florida. After completing his secondary education, he enrolled at the University of Florida supported by the Florida Undergraduate Scholarship and full-time employment at a local business. He earned a traditional 5-year engineering degree in only 4 years. In 1996, Jeff graduated with honors receiving a Bachelor of Science degree in engineering science with a concentration in biomedical engineering. He used this foundation to assist in the medical device development and clinical research programs of Computer Motion, Inc., Santa Barbara, California. In this role, Jeff was Clinical Development Site Manager for the Southeastern United States and he traveled extensively throughout the United States, Europe, and Asia collaborating with surgeons and fellow medical researchers. In 1998, Jeff married Karen, a fellow student he met during his undergraduate studies. After more than 4 years in the medical device industry, he decided to continue his academic career at the University of Florida. In 2001, Jeff began his graduate studies with a graduate research assistantship in the Computational Biomechanics Laboratory. In 2003, Jeff graduated with a perfect 4.0 GPA receiving a Master of Science degree in biomedical engineering with a concentration in biomechanics. At that time, he decided to continue his graduate education and research activities through the pursuit of a Doctor of Philosophy in mechanical engineering. In 2005, Jeff and Karen were blessed with the

birth of their first child, Jacob. Jeff would like to further his creative involvement in problem solving and the design of solutions to overcome healthcare challenges in the future.